first identified as a retinal pigment epithelium-derived protein with neuronal differentiating activity [8]. Recently, PEDF has been shown to have potent anti-angiogenic activity in cell culture and in animal models. PEDF inhibits retinal endothelial cell growth and migration, and it suppresses ischemia-induced retinal neovascularization [9]. In addition, we reported that PEDF inhibits malignant melanoma growth by suppressing tumor angiogenesis [10]. These observations led us to hypothesize that an imbalance in anti-angiogenic factors potentially involving PEDF may contribute to the pathogenesis of psoriasis. PEDF also shows anti-inflammatory activity, suggesting an additional, ameliorative role in the control of inflammation and keratinocyte proliferation.

In this study, we examined PEDF protein production in psoriasis lesions and in normal skin, and we investigated the effect of PEDF on keratinocyte proliferation in vitro and on psoriatic skin in a murine xenograft model. We also report the identification of low molecular weight PEDF peptides that show anti-angiogenic activity after topical application.

2. Experimental procedures

2.1. Patients

Sera were obtained from 21 psoriasis patients (13 males and 8 females, and mean age 46.9 years) and 14 healthy volunteers (males 7 and females 7, and mean age 42.2 years) from the Department of Dermatology, Hokkaido University Hospital. The diagnosis of psoriasis was made on the basis of clinical images and histopathological findings from skin biopsies. The enrolled patients had generalized plaque psoriasis, which were evaluated by a single qualified dermatologist. Three skin tissue specimens were obtained from each psoriatic lesion. Normal skin tissues also were obtained from healthy volunteers. Informed consent was obtained from each volunteer according to the Declaration of Helsinki Principles. All the experiments using human samples were performed under the approval of the ethical committee of Hokkaido University.

2.2. Experimental mice

The C.B-17/Icr-scid/scidJcl SCID mouse (Clea, Tokyo, Japan) was used for xenotransplantation experiments. All the animal experiments were performed under the approval of the ethical committee for animal studies in Hokkaido University.

2.3. Immunohistochemistry

The paraffin-embedded skin tissues from psoriasis patients were cut into 4 μm-thick sections. The sections were deparaffinized, incubated with 0.1% trypsin at 37 °C for 15 min. Endogenous peroxidase activity was inhibited by pretreatment with 3% hydrogen peroxide. The sections were then treated with 10% normal goat serum at room temperature for 30 min, followed by incubation with the anti-PEDF antibody (Santa Cruz Biotechnology, Santa Cruz, CA) at 4 °C overnight. After washing, the sections were incubated with horseradish peroxidase (HRP)-conjugated goat anti-rabbit IgG at room temperature for 30 min and the PEDF-positive staining visualized with diaminobenzidine (Dojin, Kumamoto, Japan) as a chromogen and hematoxylin as a counterstain.

For immunofluorescence, skin tissues were immediately embedded in optimal cutting temperature (OCT) reagent (Sakura Finetechnical, Tokyo, Japan) and snap-frozen in liquid nitrogen. Cryosections of 5 μm were prepared, washed with PBS, and then fixed in cold acetone for 10 min at −20 °C. Primary and secondary antibodies were applied at room temperature for 1 h. The sections were finally washed with PBS and mounted on microscope slides. The samples were analyzed using a Fluoview confocal laser scanning microscope (Olympus, Nagano, Japan). The following antibodies were used: rat anti-mouse CD31 antibody, anti-mouse CD3 antibody, anti-mouse Gr-1 antibody, and anti-mouse CD11b antibody (BD Biosciences, San Jose, CA), rabbit polyclonal anti-pankeratin antibody (PROGEN Biotechnik, Heidelberg, Germany), rabbit polyclonal anti-Ki67 antibody (Novocastra, Newcastle, UK), FITC-conjugated goat anti-rabbit antibody, FITC-conjugated goat anti-rat antibody (Jackson ImmunoResearch, West Grove, PA), TRITC-conjugated anti-rabbit antibody (Southern Biotechnology Associates, Birmingham, AL).

2.4. Immunoblots

Skin tissues of normal volunteers and psoriasis patients were treated with 1 M sodium hydroxide at 4 °C overnight, and the epidermal sheets easily removed from the dermal components. These tissues were frozen and then homogenized in PBS. Samples obtained from epidermis and dermis were electrophoresed on SDS–PAGE. Proteins on the gel were electrophoretically transferred to a nitrocellulose membrane (Bio-Rad, Hercules, CA) and the membranes probed with first antibody at 4 °C overnight, washed three times for 5 min, and then incubated with HRP-conjugated secondary antibodies at room temperature for 1 h. Proteins were visualized with a Konica immunostaining kit (Konica, Tokyo, Japan). The following antibodies were used: anti-PEDF and anti-VEGF rabbit polyclonal antibody (Santa Cruz Biotechnology), anti-α-tubulin mouse monoclonal antibody (Sigma, St. Louis, MO), HRP-conjugated goat anti-rabbit IgG, and HRP-conjugated goat anti-mouse IgG (Biosource, Camarillo, CA). We used anti-PEDF at 1:200, and the secondary antibodies at 1:1000 dilutions.

2.5. RT-PCR analysis

RNA (0.5 μg) was used to produce cDNA using a reverse transcription kit (Sigma, Poole, Dorset, United Kingdom). PCR was done using a 2400 thermocycler (Perkin-Elmer, Norwalk CT) with conditions set to 40 s at 94 °C, 60 s at 55 °C, and 60 s at 72 °C (30 cycles). The quality of DNA was verified by 0.59 kb β-actin PCR products using primers (forward 5′-ATGATATCGCCGCGCTCGTC-3′; reverse 5′-CGCTCGGTGAGGATCTTCA-3′). PEDF forward and reverse primers were 5′-GGTGCTACTCCTCTGCATT-3′ and 5′-ACTGAACCTGACCGTACAAGAAAGGATCCTCCTCCTC-3′. PCR products were separated by 2% agarose gel and visualized under UV light following ethidium bromide staining.

2.6. Preparations of PEDF proteins

The PEDF proteins were purified as described previously [9]. Briefly, 293T cells (ATCC, Rockville, MD, USA) were transfected with the recombinant vector pBK-CMV-C terminally hexahistidine-tagged PEDF using FuGENE® 6 transfection reagent (Roche Diagnostics, Mannheim, Germany) according to the manufacturer's instructions. The PEDF proteins were purified from conditioned media by a Ni-NTA spin kit (Qiagen, Hilden, Germany) according to the manufacturer's recommendation. Sodium dodecyl sulphate–polyacrylamide gel electrophoresis (SDS–PAGE) of purified PEDF proteins revealed a single band with a molecular mass of about 50 kDa, which showed positive reactivity with monoclonal antibodies directed against human PEDF (Transgenic, Kumamoto, Japan).

2.7. PEDF enzyme-linked immunosorbent assay

A PEDF enzyme-linked immunosorbent assay was performed as previously reported [11]. Briefly, a 96-well microtiter plate (Nalge

Nunc International, Rochester, NY) was coated by overnight incubation with anti-PEDF monoclonal antibody (Transgenic, Kumamoto, Japan). Samples were diluted 50-fold in 10 mM PBS pH 7.4, 0.25% BSA and 0.05% Tween-20, and then incubated at room temperature for 2 h. After washing, a biotinylated anti-human PEDF polyclonal antibody (R&D Systems, Minneapolis, MN) was added and incubation continued for 2 h at room temperature. The plate was then incubated with HRP-conjugated streptavidine solution (Zymed, South San Francisco, CA) at room temperature for 30 min. After washing, the chromogenic substrate solution (Dako, Tokyo, Japan) was added and the plate was incubated at room temperature for 15 min. Optical densities were measured at 450 nm and protein concentrations calculated from a standard curve generated by a curve-fitting program (Berthold Technology, Bad Wildbad, Germany).

2.8. PEDF secretion from cultured keratinocytes and fibroblasts

Normal human epidermal keratinocytes (NHEKs) were purchased from Clontech (Mountain View, CA and cultured in KGM® medium (Cambrex, East Rutherford, NJ) until 70% confluence. Normal human fibroblasts were purchased from Dainippon Seiyaku (Osaka, Japan) and cultured in Dulbecco's Modified Eagle's Medium (DMEM) (Invitrogen, Carlsbad, CA) containing 10% FBS, 1% penicillin, 1% streptomycin and 1% amphotericin B until 70% confluence. The cells were expanded in 12 cm sterile culture dish with 10 ml of medium, and then stimulated with lipopolysaccharide (Sigma) at 37 °C for 72 h. Media was collected 1 day after stimulation. PEDF concentrations in collected medium were assessed by ELISA as described above.

2.9. Keratinocyte proliferation assay

NHEKs were seeded into 96-well plates at a concentration of 10^3 cells in 100 μl of medium per well. After cultivation with 1, 10, 100 nM recombinant PEDF [12] and/or 100 ng/ml recombinant VEGF (R&D systems) for 2 and 4 days, 10 μl of Cell Counting Kit (Dojin) was added to each well. After incubation for 2 h, the absorbance at 450 nm was measured on a microplate reader.

2.10. Treatment of the grafted skin lesions with recombinant PEDF

A graft bed of approximately 1 cm^2 was created on the shaved area of the back of a 7 to 8-week-old anesthetized SCID mouse by removing the full-thickness skin and keeping the vessel plexus intact on the fascia overlying back muscles. The human skin obtained by biopsy was washed in PBS containing 1% penicillin, 1% streptomycin and 1% amphotericin B, and fatty deposits were removed by gentle dissection. The full-thickness human skin graft was placed onto wound bed. The transplants were held in place using 5/0 silk suture material, and 1% gentamicin sulfate ointment was applied. The graft was covered with an adhesive wound

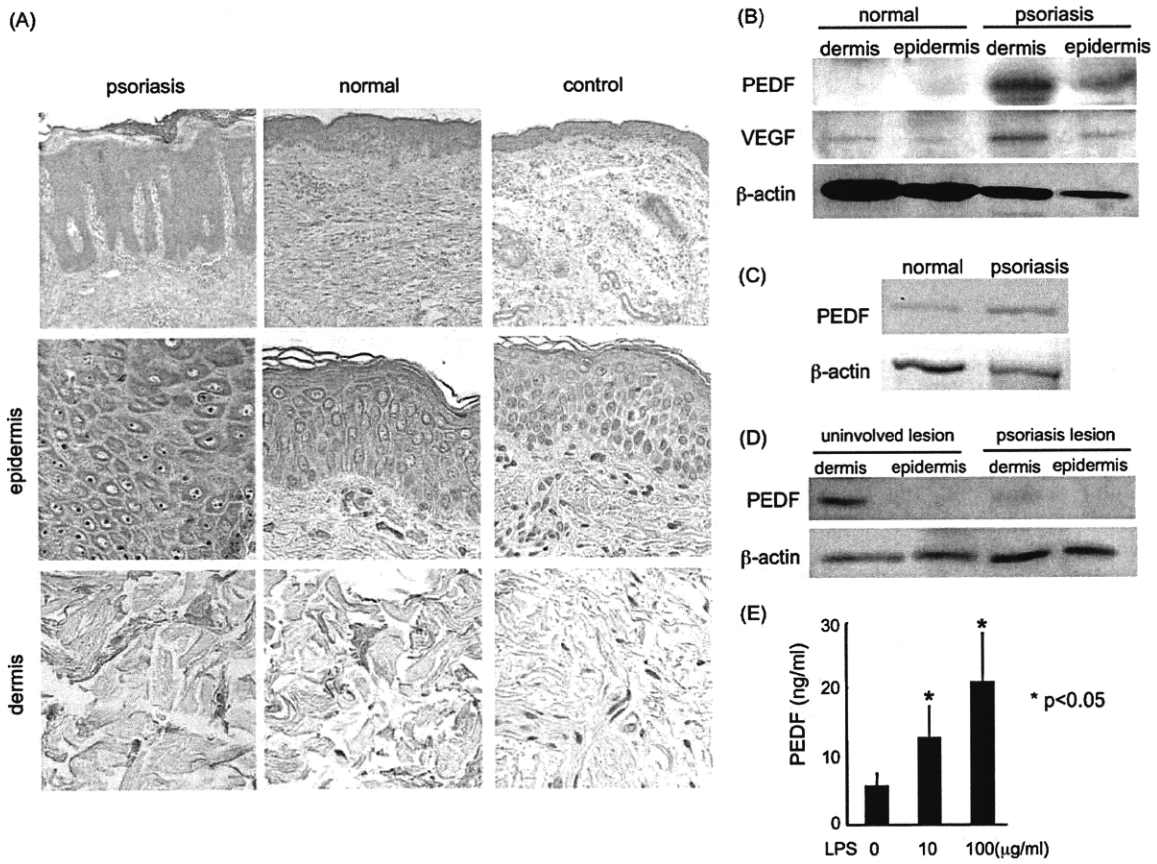

Fig. 1. PEDF is expressed in both the epidermis and dermis. (A) Immunohistochemistry of normal and psoriatic skin lesions. In normal skin, PEDF was detected in both the epidermis and the dermis. PEDF was significantly up-regulated in psoriatic epidermis in comparison with normal epidermis. (B) The expression of PEDF protein was up-regulated in psoriasis lesions. Positive bands were identified with a molecular weight of about 50 kDa from both the epidermis and dermis, which corresponds to the molecular weight of PEDF. (C) PEDF mRNA levels were analyzed using RT-PCR. The expression of PEDF mRNA was slightly up-regulated in psoriasis lesions compared to that of normal skin. (D) The expression of PEDF protein was up-regulated in uninvolved lesion of psoriasis patient compared to psoriasis lesion. (E) The levels of PEDF in the supernatants of cultured normal human keratinocytes were assessed by ELISA. LPS (10 or 100 μg/ml) was used to stimulate keratinocyte production of PEDF (*$p < 0.05$).

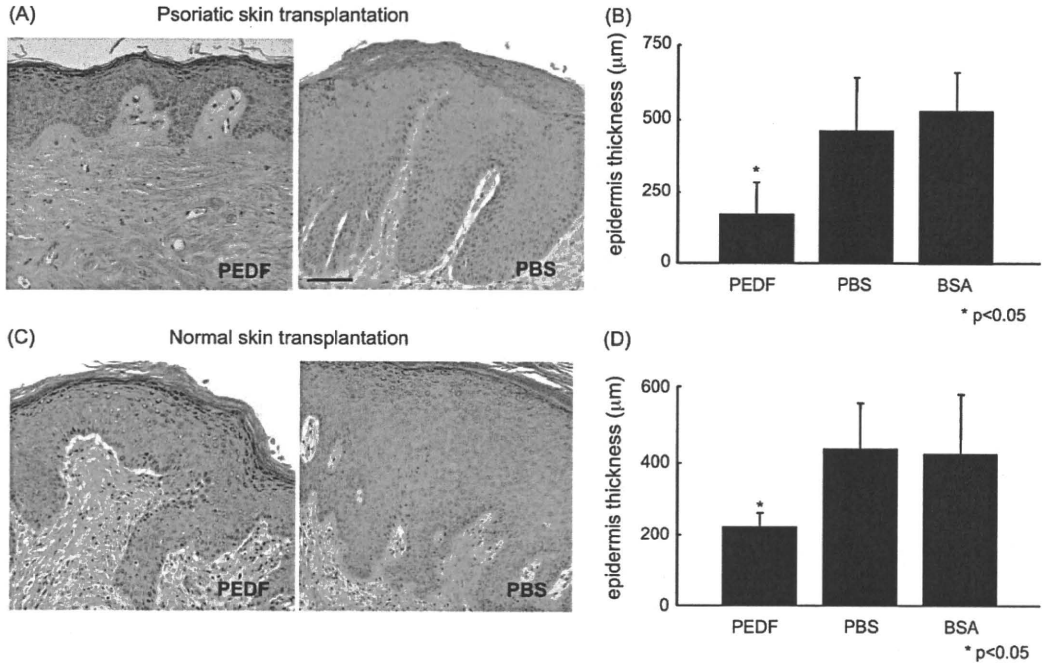

Fig. 2. Intradermal PEDF administration reduced the thickness of grafted epidermis in xenotransplanted SCID mice. Acanthosis was significantly reduced both in psoriatic (A, B) and normal (C, D) skin when compared to PBS or BSA injected groups. Scale bar, 50 μm. Values shown are means and SDs based on four to six measurements per histological section in four histological sections per mouse from duplicate mice transplanted with skin samples from four donors (*$p < 0.05$).

dressing and then with a standard bandage. Dressing material and sutures were removed 7 days after transplantation.

Grafted mice received recombinant PEDF in 50 μl of PBS by intradermal injection around the xenograft lesion at 30 μg/mouse every three days for three weeks. The PEDF dose was well tolerated without any evident side effects. Mice in the control group received the same volume of PBS or BSA (30 μg). The day after the last injection, biopsies were collected from the transplants from both treatment and control groups. The skin tissues were immediately embedded in OCT reagent and snap-frozen in liquid nitrogen. Cryosections of 5 μm were then prepared for histological and immunohistochemical staining.

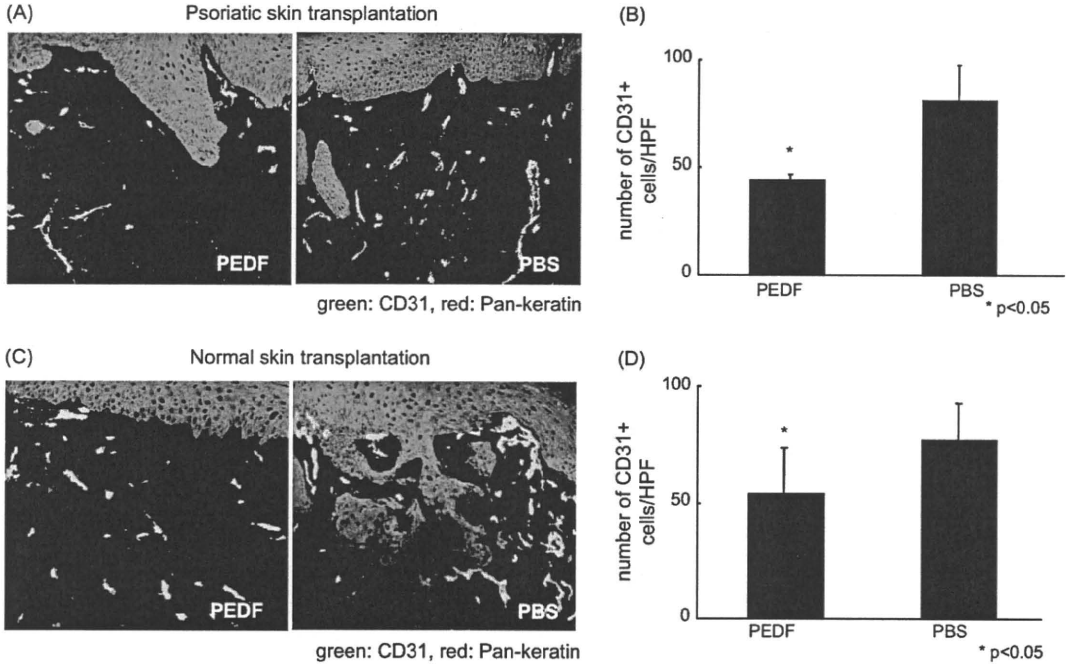

Fig. 3. Intradermal PEDF administration reduced angiogenesis of grafted epidermis. CD31-positive cells (capillary endothelial cells) were enumerated by immunofluorescence after the treatment of psoriatic (A, B) and normal skin (C, D) with PEDF or PBS. Quantification of CD31-positive blood vessels per 100× microscopic field in human skin grafted areas. The data are presented as mean CD31-positive blood vessel numbers per 100× microscopic field, ±SD (*$p < 0.05$).

2.11. Identification of functional PEDF peptides

Full-length human PEDF cDNA was divided into three parts. Polymerase chain reaction (PCR) products digested by NdeI and SalI were ligated into the multiple cloning site of expression vector pGEX-6P-1 (Amersham Biosciences, Buckinghamshire, United Kingdom). Sequences of the sense and antisense primers were: 5′-AAACATATGCAGGCCCTGGTGCTACTCCTCTGCAT-3′ and 5′-CCCGTCGACTTATGACTTTTCCAGAGGTGCCACAAA-3′ for amplifying F1 cDNA fragment, 5′-AAACATATGTATGGGACCAGGCCCAGAGTCCTGA-3′ and 5′-CCCGTCGACTTAGTCATGAATGAACTCGGAGGTGA-3′ for F2, and 5′-GGGCATATGATAGACCGAGAACTGAAGACCGTGCA-3′ and 5′-AAAGTCGACTTAGGGGCCCCTGGGGTCCAGAAT-3′ for F3. Each human PEDF fragment was purified according to the method of Walker et al. [13]. Human PEDF peptides (see Fig. 6) were synthesized (Sigma–Aldrich, Tokyo, Japan). MG63 human osteosarcoma cells (Health Science Research Resources Bank, Tokyo, Japan) were maintained in Dulbecco's modified Eagle's medium (DMEM) supplemented with 10% of fetal bovine serum (FBS) (ICN Biomedicals Inc., Aurora, OH, USA) and 100 units/ml penicillin/streptomycin. PEDF fragment or peptide treatment was carried out in a medium containing 0.1% of FBS. HUVECs and MG63 cells were treated with or without 100 nM PEDF protein, fragments (F1–F3) or peptides (P1–P6, P5–1, P5–2, and P5–3) or VEGF (25 ng/ml) for 24 h. HUVECs additionally were treated with 100 ng/ml recombinant VEGF (R&D systems) for 2 and 4 days. Cells were incubated with [^{3}H]thymidine (Amersham Bioscience) or 5-bromo-2′deoxyuridine (BrdU) (Roche, Basel, Switzerland) for the last 4 h of culture and proliferation assessed as described previously [14,15].

For the analysis of p21 production, 50 μg of whole cell lysates were prepared and assayed for the expression of p21 and β-actin by Western blotting. Reaction with antibodies and detection with an enhanced chemiluminescence detection system (Amersham Biosciences) were performed as described previously [16].

2.12. Skin penetration of topical applied PEDF peptide

Biotin-labeled PEDF peptide (Sigma–Aldrich) was dissolved in PBS (1 mM) and 70 μl applied to the mouse skin. After 2 h, the applied site was removed and localization in the skin was determined by rhodamine–avidin staining (BD Biosciences). CD31 staining (BD Biosciences) was performed simultaneously and the samples analyzed using a Fluoview confocal laser scanning microscope (Olympus). The experiments of peptide application were repeated 3 times, and 3 mice were used in each experiment.

2.13. Treatment of the grafted psoriatic lesions with PEDF peptide

PEDF peptide was dissolved in PBS (1 mM) and 70 μl of the solution was applied on the grafted site daily for 14 days. No side effects were apparent at the applied sites. Mice in the control group received the same volume of PBS. Biopsies were collected on the day following the last injections and analyzed as described above.

2.14. Statistical analysis

Data were analyzed using unpaired, 2-tailed Student's *t* test. A *p* value less than 0.05 was considered significant.

3. Results

3.1. PEDF is highly expressed in epidermal psoriasis lesions

Immunohistochemical analysis revealed that PEDF protein is present in the cytoplasm of keratinocytes of both psoriatic and normal skin (Fig. 1A). In the dermis, fibroblasts also were positive for PEDF, but the staining was less intense than in the epidermis. Western blotting analysis of human epidermal and dermal proteins revealed a single band with a molecular weight of about 50 kDa (Fig. 1B). PEDF protein and mRNA levels were significantly higher in psoriasis lesions when compared to normal skin (Fig. 1C).

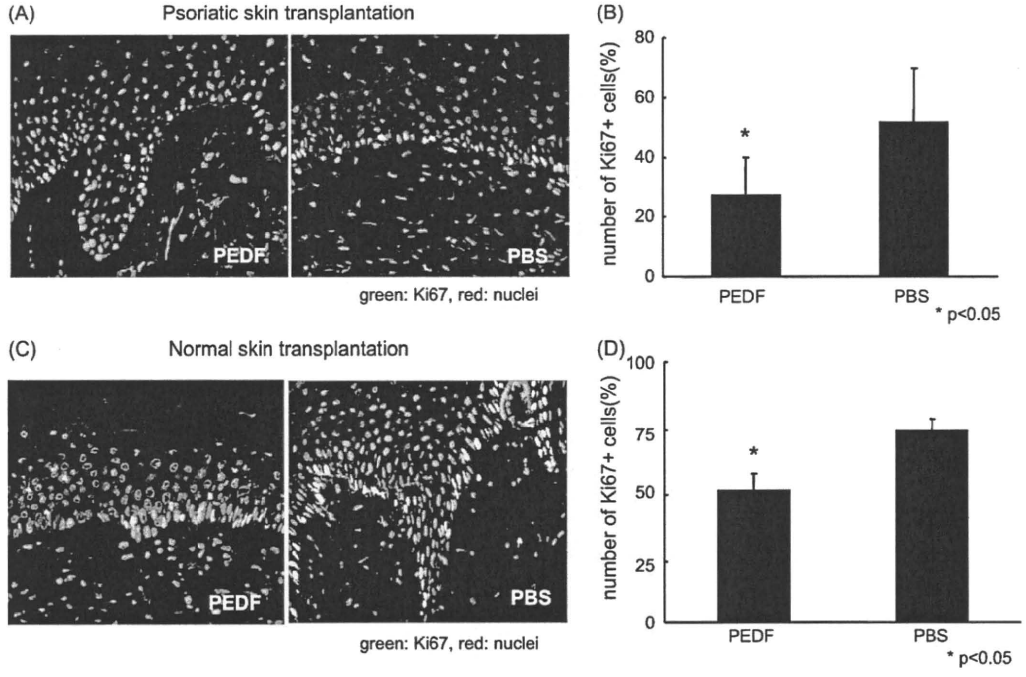

Fig. 4. Epidermal proliferation in basal keratinocytes is inhibited by PEDF. Ki-67-positive (proliferating) cells were stained and enumerated by immunofluorescence after the treatment of psoriatic (A, B) and normal skin (C, D) with PEDF or PBS. The Ki-67-positive keratinocytes in the basal layer were enumerated and the percentage of Ki-67-positive cells in basal layer calculated (*$p < 0.05$).

Interestingly, PEDF protein levels of uninvolved lesion of psoriasis patient were higher than that in psoriasis lesions (Fig. 1D). VEGF also was increased in psoriatic skin, which is consistent with prior reports [6].

3.2. PEDF secretion from cultured keratinocytes after lipopolysaccharide stimulation

PEDF was constitutively secreted by cultured keratinocytes (Fig. 1E) and after LPS stimulation, its secretion was significantly up-regulated in a dose-dependent manner ($p < 0.05$). Fibroblasts by contrast failed to show up-regulation of PEDF secretion after LPS or IL-1β stimulation (data not shown). These results imply that keratinocytes but not fibroblasts secrete PEDF in a regulated fashion in response to inflammatory stimulation. These data contrast with a prior report that PEDF is detected primarily in the dermis, with little protein evident in the epidermal layers [17].

3.3. PEDF levels in serum of psoriasis patients and normal controls

Serum VEGF levels have previously been reported to be significantly elevated in psoriasis patients [6]. If elevated serum VEGF values reflect cytokine overproduction in the skin that then enters the systemic circulation, the pathogenesis in psoriasis might relate not only to a disruption of local angiogenesis in the skin but also to angiogenesis at the systemic level. We next examined whether serum PEDF serum levels also were elevated in psoriasis patients, however we observed no significant difference in PEDF levels between psoriasis patients (14.9 ± 4.1 μg/ml) ($n = 21$) and normal controls (15.1 ± 2.9 μg/ml) ($n = 14$). Furthermore there is no correlation between psoriasis severity and serum PEDF concentration.

3.4. Intradermal injection of PEDF reduces acanthosis, dermal angiogenesis and keratinocyte proliferation of grafted skin by

We hypothesized that PEDF produced by keratinocytes not only regulates local angiogenesis, but also suppresses epidermal proliferation and the resulting acanthosis in psoriatic inflammatory lesions. To investigate this possibility *in vivo*, we studied a psoriasis graft model in which patient-derived skin is xenografted onto severe combined immunodeficient (SCID) mice. Recombinant PEDF (30 μg) was injected intradermally in the area of the graft for three weeks and epidermal thickness evaluated histopathologically. The epidermal thickness of the grafted area was significantly reduced after treatment with PEDF when compared to BSA or PBS treated controls (Fig. 2). Injections of equivalent amounts of BSA, as a non-specific protein control, did not reduce epidermal thickness. Normal human skin transplanted to SCID mice also showed a reduction of epidermal thickness after PEDF-treatment. On the

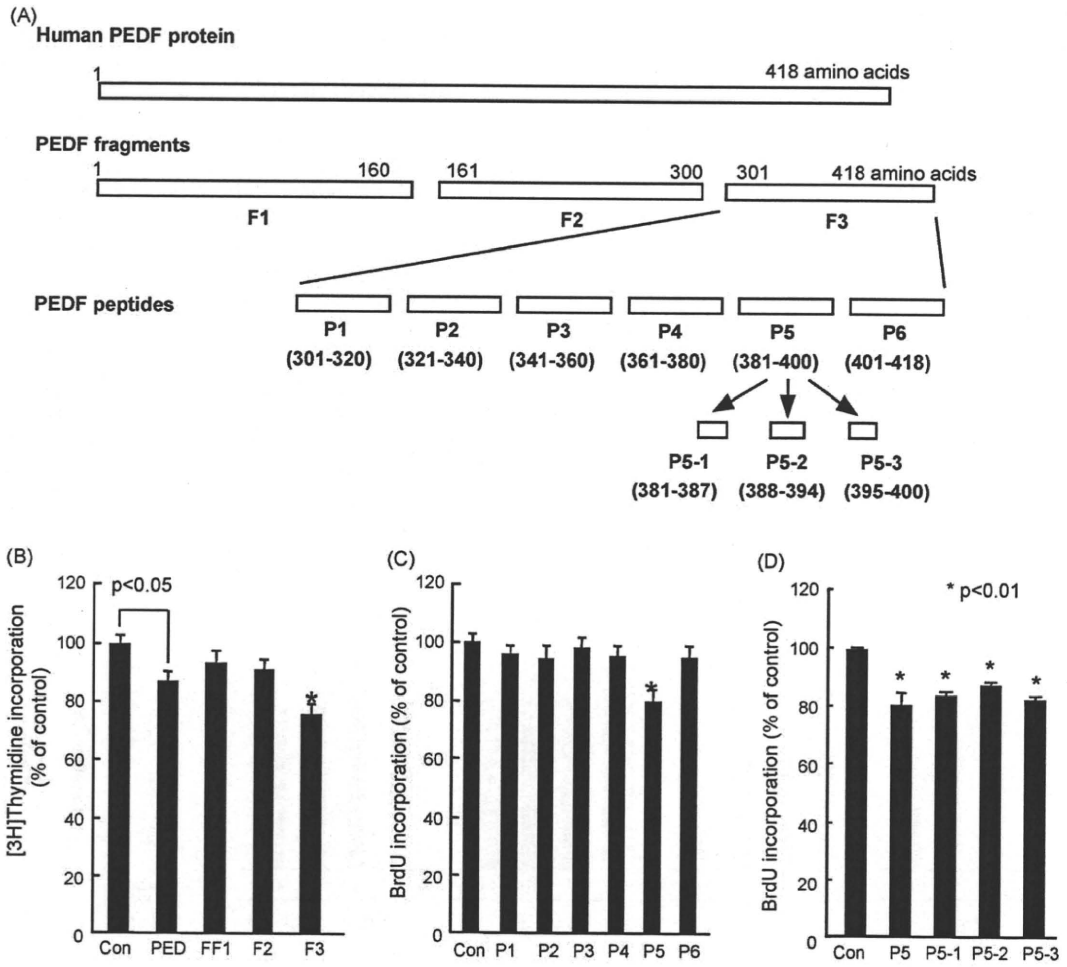

Fig. 5. Anti-angiogeneic activity of PEDF peptides. Diagram of the PEDF peptides studied for their effect on the growth of MG63 cells (B–D) or HUVEC (E). MG63 cells or HUVEC were treated with or without 100 nM PEDF, fragments or peptides and then [^{3}H]thymidine (B) and BrdU incorporation into the cells (C, D) were measured. The percentage of [^{3}H]thymidine or BrdU incorporation is indicated on the ordinate and related to the value of the control. *$p < 0.01$ compared to the value with 100 nM PEDF protein.

other hand vacuolar structure can be seen in basement membrane on normal skin plantation stimulated with PEDF. We previously reported cytotoxic effect of PEDF. PEDF directly induce tumor cell apoptosis via Fas–FasL interaction [10]. Therefore PEDF affects epidermis resulting vacuolization of dermal–epidermal junction. Normal skin underwent more hyperproliferative response after transplantation compared to psoriatic skin as previous reports [18,19]. The mechanism underlying the hyperplastic response in normal skin after transplantation is unknown at present. Some degree of epidermal hyperplasia is often seen as part of the wound-healing response in the skin. Perhaps one or more growth factors present in the healing murine skin is responsible for triggering proliferation of epidermal keratinocytes in the transplanted human tissue [19].

To evaluate the effects of PEDF on angiogenesis and epidermal proliferation in this *in vivo* model, we enumerated the CD31+ capillary endothelial cells in the superficial dermis and the Ki-67+ proliferating keratinocytes by immunofluorescence. The number of CD31 positive capillary endothelial cells in the papillary dermis was significantly reduced after PEDF treatment (Fig. 3) in both psoriasis and normal skin grafts. The frequency of proliferating Ki-67-positive cells in the basal cell layer also was significantly reduced after PEDF treatment (Fig. 4).

Since inflammatory cell infiltration is considered important in the pathogenesis of psoriasis (refs), it is possible that the reduction of epidermal thickening or acanthosis is due to the inhibition of inflammatory cell infiltration. However, the number of T cells (CD3+), neutrophils (Gr-1+) and monocytes (Cd11b+) in the superficial dermis were not statistically different between the treated and un-treated group (*data not shown*).

3.5. Improvement of clinical and histologic features of psoriasis by topical application of PEDF peptide

Although intact skin is impermeable to many bio-molecules such as proteins, compounds less than 1 kDa in mass may pass transcutaneously. Moreover, inflammatory changes in the skin, as occur in psoriasis, frequently lead to reduced barrier function due to aberrant epidermal cell differentiation and alterations in ceramide content [20,21]. We thus considered that psoriasis skin lesions may be amenable to topical application of low molecular weight, PEDF-derived peptides [22].

To identify potential PEDF peptides that might exhibit anti-psoriatic properties, we screened peptides derived from the proteolytic fragmentation of PEDF for their anti-proliferative action on MG63 cells, which previously have been shown to be sensitive to the growth inhibitory action of PEDF [14]. As shown in Fig. 5A and B, PEDF fragment F3, but not F1 or F2, significantly inhibited the growth of MG63 cells at concentrations comparable to intact PEDF protein (Fig. 5B). The PEDF-derived peptide, P5 also exhibited an anti-proliferative properties on MG63 cells (Fig. 5C). P5–1 (381–387, MW: 841), P5–2 (388–393, MW: 770) or P5–3 (388–393, MW: 770) peptides had similar growth-inhibitory activity when compared with the P5 peptide (Fig. 5D).

To investigate the inhibitory activity of PEDF peptides on angiogenesis, we first assessed endothelial tube formation *in vitro*. P5–2 and P5–3 but not P5–1 showed significant inhibitory effects on tube formation (Fig. 6A). The active PEDF peptides inhibited endothelial tube formation concentrations of 100 and 500 nM. To investigate the cooperative effects of VEGF and PEDF, we added PEDF peptide and VEGF simultaneously in endothelial tube formation assay. P5–2 and P5–3 but not P5–1 normalized VEGF-induced tube formation (Fig. 6A). All of these peptides also inhibited the proliferation of endothelial cells (Fig. 6B), however this suppressive effect was in concentrations that were in the μM range. We and others have previously reported that PEDF inhibits VEGF-stimulated endothelial cell proliferation, whereas only PEDF has only a minimal effect on endothelial cell proliferation in the absence of VEGF stimulation [9,14]. Therefore PEDF peptides might be required to be present in high concentration to inhibit endothelial cell proliferation. A peptide control with the same amino acid content and a randomized sequence did not show any effect. PEDF has been reported to suppress VEGF-stimulated endothelial proliferation via cell cycle inhibition [23]. We therefore

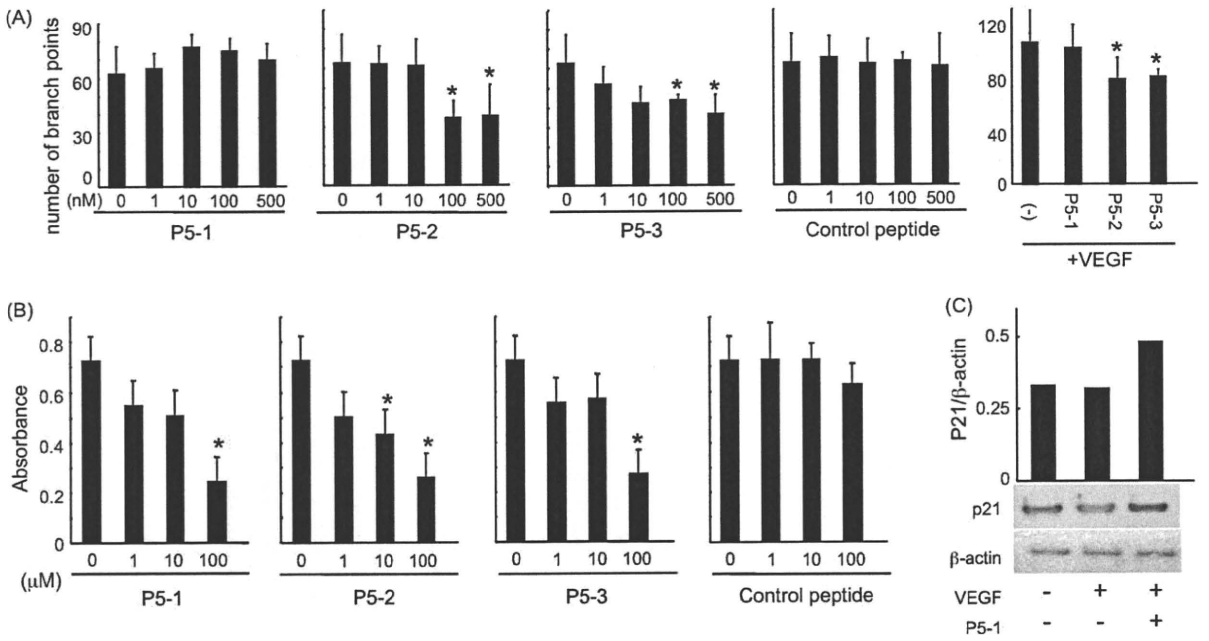

Fig. 6. (A) The endothelial tube formation assay. PEDF 1–3 showed a level of anti-angiogenic activity comparable to recombinant PEDF (*$p < 0.05$). (B) Diagram of the PEDF peptides studied for their effect on the growth of HUVEC. HUVEC were treated with or without 100 nM PEDF, fragments or peptides and then BrdU incorporation into the cells was measured. The percentage of BrdU incorporation is indicated on the ordinate and related to the value of the control. *$p < 0.01$ compared to the value with no addition.

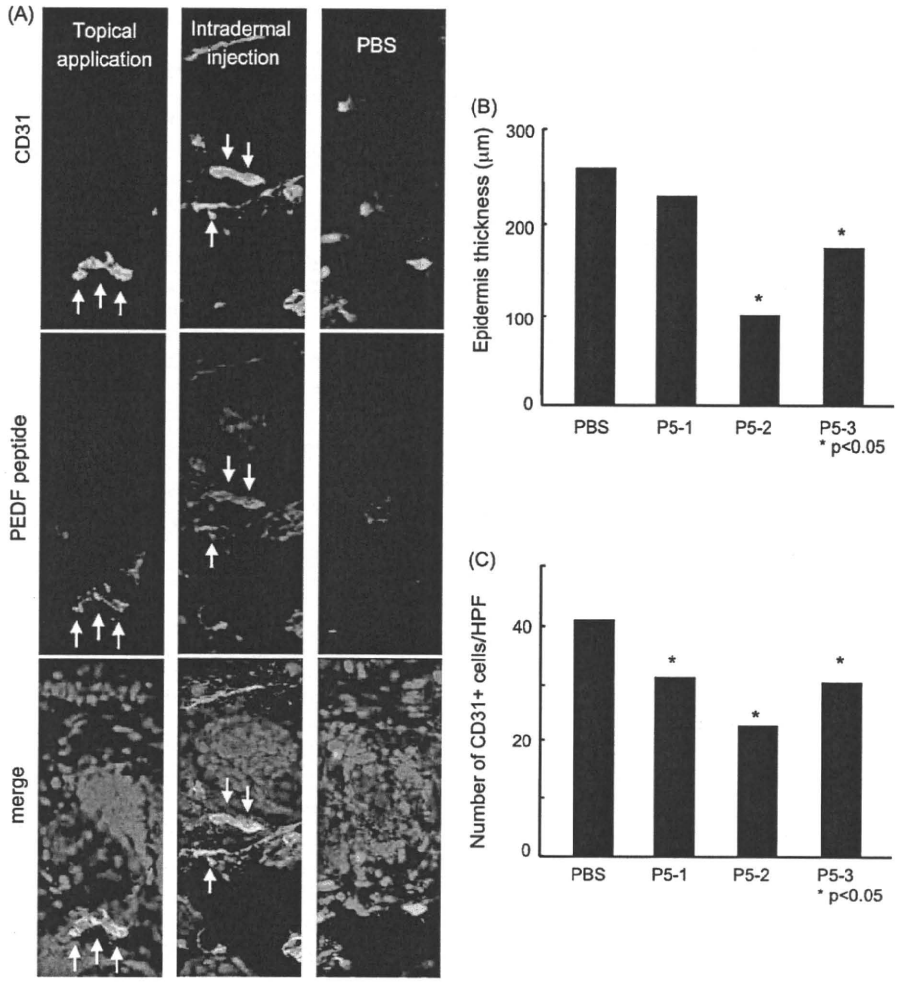

Fig. 7. Topically applied PEDF peptides penetrate into skin and reduce epidermal thickness and angiogenesis. (A) Biotin-labeled PEDF peptide (P5–1) was applied to the skin and its localization studied 2 h later using rhodamine–avidin staining as described in Section 2. Co-localization with PEDF peptide and endothelial cells (CD31+) is indicated by the arrows. The P5–2 and P5–3 also penetrated into the skin (*data not shown*). (B) Local application of PEDF peptide reduced thickness of grafted epidermis in xenotransplanted SCID mice. (*$p < 0.05$). (C) CD31-positive cells (capillary endothelial cells) were enumerated by immunofluorescence. The PEDF-treated group showed significantly reduced number of CD31+ cells (*$p < 0.05$).

analyzed the expression of the p21, cyclin-dependent kinase inhibitor [16]. PEDF peptide increased the expression of p21, suggesting that its inhibitory effect is mediated at least in part via p21 induction (Fig. 6C).

We next examined whether PEDF-derived peptides penetrate into the skin. Biotin-labeled PEDF peptide was applied to murine skin and its localization analyzed 2 h later using rhodamine–avidin staining. The PEDF peptide was detected in the dermis and co-localized with endothelial cells (Fig. 7A); the staining pattern was similar to that observed after the intradermal injection of the peptide. In addition, endothelial cells express PEDF receptor [24]. Therefore PEDF peptides might colocalize with endothelial cells.

Finally, we assessed the therapeutic potential of PEDF peptides after their topical application to human psoriatic skin grafted onto SCID mouse. PEDF peptides were dissolved in PBS (1 mM) and 70 μl of peptide applied to the grafted site each day for 10 days. Mice in the control group received the same volume of PBS. After two weeks of treatment, the epidermal thickness of the grafted area was significantly reduced in the P5–2 and P5–3-treated group (Fig. 7B). The number of CD31-positive capillary endothelial cells in the papillary dermis was significantly reduced in the all PEDF peptide-treated groups (Fig. 7C).

4. Discussion

In this study, we demonstrate that PEDF is produced both within the human epidermis and dermis, and that significantly higher levels are present in the psoriatic epidermis. Cultured keratinocytes and fibroblasts constitutively secrete PEDF; however, incubation with the model inflammatory stimulus LPS increases PEDF production only by keratinocytes. In addition, the local administration of PEDF reduces both acanthosis in psoriasis lesions and the hyperplasia of normal skin in a xenograft transplant model. This effect appeared to due to the inhibition of dermal capillary angiogenesis and epidermal proliferation. Finally, we identified a low-molecular weight, anti-angiogenetic PEDF peptide showed that its topical application reduced the proliferative and inflammatory features of psoriatic lesions.

Inappropriate angiogenesis has been proposed to contribute to the pathogenesis of psoriasis [4,5], although the precise cellular and molecular basis for this response remains unclear. Angiogenic processes are regulated by a delicate balance of pro-angiogenic and anti-angiogenic factors [25]. Under conditions such as tumor formation, wound healing, and possibly psoriasis, the positive regulators of angiogenesis predominate and vascular endothelial

cells become activated. In psoriasis, angiogenic factors such as VEGF are up-regulated and anti-angiogenic factors such as PEDF are simultaneously up-regulated to maintain a homeostatic balance. However, the overexpression of angiogenic factors may overcome and surmount this balance in psoriasis, resulting an acceleration of angiogenesis [4,5].

Interestingly, the level of PEDF protein in uninvolved lesions was observed to be much higher than that in psoriatic lesions. These data suggest that the angiogenic balance is maintained by an up-regulated expression of PEDF in uninvolved lesions, whereas insufficient up-regulation of PEDF may contribute to the psoriatic phenotype. The regulation of PEDF may be an innate feature of psoriasis rather than a consequence of inflammation.

We found no significant differences in the serum levels of PEDF between psoriatic patients and normal controls. A previous report has suggested that circulating PEDF has the capacity to inhibit angiogenesis at the systemic level [23]. Our investigations showed that PEDF is up-regulated in the psoriatic epidermis, which likely affects the local microenvironment; however, local PEDF production by keratinocytes was not sufficient to lead to an increase in the serum concentration of this mediator. We hypothesize that VEGF levels in psoriatic skin may overcome the inhibitory action of PEDF on angiogenesis, resulting in a pro-angiogenic switch in the microenvironment around psoriasis lesions. In cultured keratinocytes, PEDF is up-regulated by LPS stimulation, suggesting that PEDF production by keratinocytes might occur in response to inflammatory activation.

We showed herein that PEDF was detected in both the epidermis and dermis, which contrasts with a previous paper that reported that PEDF was only detected in dermal layers, and not in normal epidermis [17]. In our immunohistochemical studies, PEDF was highly expressed in psoriatic keratinocytes, although the normal, steady-state epidermis showed only weak staining. We confirmed that PEDF is secreted by cultured keratinocytes and induced LPS stimulation, suggesting that PEDF production by keratinocytes might depend on inflammatory activation. By contrast, cultured fibroblasts constitutively secrete PEDF regardless of LPS activation. Accordingly, we hypothesize that fibroblasts are major contributors to PEDF production under normal conditions, and that keratinocytes contribute to PEDF production in certain inflammatory conditions.

A receptor for PEDF has been recently reported [24], however we could not detect the expression of this protein in keratinocytes using RT-PCR (*data not shown*). Because PEDF has not only anti-angiogenic but also anti-proliferative effects on many cell types, we speculate that PEDF may interact with multiple receptors in addition to the one previously reported. It has been reported that the anti-angiogenic effects of PEDF reside in the N-terminus within residues 24–57, which is distinct from the sequence we report herein [26]. Residues 24–57 are included in the F1 fragment of PEDF in the present study, however F1 did not show the inhibitory activity of PEDF (Fig. 5). We nevertheless were successful in identifying low-molecular weight peptides (MW < 850 Da) that penetrate the skin and show a significant anti-angiogenic effect in vitro and in vivo.

We demonstrated that acanthosis of human psoriatic skin was significantly reduced by local administration of PEDF in a mouse xenograft model, and that this effect appeared due to reduced angiogenesis and basal cell proliferation. These results suggest that a PEDF-based, topical therapeutic might be an effective therapy for psoriasis. We identified PEDF peptides with molecular weights <850 Da that penetrate the skin and showed these peptides to have anti-angiogenic activity and to reduce psoriatic epidermal hyperplasia. In addition, drug delivery system is one of the most critical issue about clinical application. Small peptide is rapidly degraded in vivo, so we have to develop a slow-release system such as biodegradable gelatin microspheres.

In conclusion, these studies provide the first report of a role for PEDF in the pathogenesis of psoriasis. Furthermore, low molecular weight peptides derived from PEDF show anti-angiogenic activity in psoriatic skin in an *in vivo* model of disease, and may offer a novel therapeutic approach for the treatment of psoriasis.

Acknowledgements

We thank Ms. Yuika Osaki for her excellent technical assistance and Prof. James R. McMillan for his manuscript proofreading.

References

[1] Schon MP, Boehncke WH. N Engl J Med 2005;352:1899–912.
[2] Bowcock AM, Krueger JG. Nat Rev Immunol 2005;5:699–711.
[3] Creamer JD, Barker JN. Clin Exp Dermatol 1995;20:6–9.
[4] Detmar M, Brown LF, Claffey KP, Yeo KT, Kocher O, Jackman RW, et al. J Exp Med 1994;180:1141–6.
[5] Ballaun C, Weninger W, Uthman A, Weich H, Tschachler E. J Invest Dermatol 1995;104:7–10.
[6] Bhushan M, McLaughlin B, Weiss JB, Griffiths CE. Br J Dermatol 1999;141:1054–60.
[7] Lowes MA, Bowcock AM, Krueger JG. Nature 2007;445:866–73.
[8] Tombran-Tink J, Chader GG, Johnson LV. Exp Eye Res 1991;53:411–4.
[9] Dawson DW, Volpert OV, Gillis P, Crawford SE, Xu HJ, Benedict W, et al. Science 1999;285:245–8.
[10] Abe R, Shimizu T, Yamagishi S-i, Shibaki A, Amano S, Inagaki Y, et al. Am J Pathol 2004;164:1225–32.
[11] Amano S, Yamagishi S-i, Inagaki Y, Nakamura K, Takeuchi M, Inoue H, et al. Microvasc Res 2005;69:45–55.
[12] Yamagishi S, Inagaki Y, Amano S, Okamoto T, Takeuchi M, Makita Z. Biochem Biophys Res Commun 2002;296:877–82.
[13] Walker PA, Leong LE, Ng PW, Tan SH, Waller S, Murphy D, et al. Biotechnology (N Y) 1994;12:601–5.
[14] Takenaka K, Yamagishi S-i, Jinnouchi Y, Nakamura K, Matsui T, Imaizumi T. Life Sci 2005;77:3231–41.
[15] Fukami K, Ueda S, Yamagishi S-i, Kato S, Inagaki Y, Takeuchi M, et al. Kidney Int 2004;66:2137–47.
[16] Brizzi MF, Dentelli P, Pavan M, Rosso A, Gambino R, Grazia De Cesaris M, et al. J Clin Invest 2002;109:111–9.
[17] Francis MK, Appel S, Meyer C, Balin SJ, Balin AK, Cristofalo VJ. J Invest Dermatol 2004;122:1096–105.
[18] Bhagavathula N, Nerusu KC, Fisher GJ, Liu G, Thakur AB, Gemmell L, et al. Am J Pathol 2005;166:1009–16.
[19] Zeigler M, Chi Y, Tumas DB, Bodary S, Tang H, Varani J. Lab Invest 2001;81:1253–61.
[20] Nickoloff BJ, Nestle FO. J Clin Invest 2004;113:1664–75.
[21] Segre JA. J Clin Invest 2006;116:1150–8.
[22] Bos JD, Meinardi MMHM. Exp Dermatol 2000;9:165–9.
[23] Doll JA, Stellmach VM, Bouck NP, Bergh ARJ, Lee C, Abramson LP, et al. Nat Med 2003;9:774–80.
[24] Notari L, Baladron V, Aroca-Aguilar JD, Balko N, Heredia R, Meyer C, et al. J Biol Chem 2006;281:38022–37.
[25] Distler JH, Hirth A, Kurowska-Stolarska M, Gay RE, Gay S, Distler O. Q J Nucl Med 2003;47:149–61.
[26] Filleur S, Volz K, Nelius T, Mirochnik Y, Huang H, Zaichuk TA, et al. Cancer Res 2005;65:5144–52.

RESEARCH ARTICLE

Human Mutation

OFFICIAL JOURNAL
HGVS
HUMAN GENOME VARIATION SOCIETY
www.hgvs.org

Prevalent *LIPH* Founder Mutations Lead to Loss of P2Y5 Activation Ability of PA-PLA$_1\alpha$ in Autosomal Recessive Hypotrichosis

Satoru Shinkuma,[1] Masashi Akiyama,[1]* Asuka Inoue,[2] Junken Aoki,[2] Ken Natsuga,[1] Toshifumi Nomura,[1,3] Ken Arita,[1] Riichiro Abe,[1] Kei Ito,[1] Hideki Nakamura,[1] Hideyuki Ujiie,[1] Akihiko Shibaki,[1] Hiraku Suga,[4] Yuichiro Tsunemi,[4] Wataru Nishie,[1] and Hiroshi Shimizu[1]

[1]Department of Dermatology, Hokkaido University Graduate School of Medicine, Sapporo 060-8638, Japan; [2]Graduate School of Pharmaceutical Sciences, Tohoku University, Sendai 980-8578, Japan; [3]Epithelial Genetics Group, Division of Molecular Medicine, Colleges of Life Science and Medicine, Dentistry & Nursing, University of Dundee, Dundee, DD1 5EH, United Kingdom; [4]Department of Dermatology, Tokyo University, Faculty of Medicine 113-8655, Tokyo, Japan

Communicated by David S. Rosenblatt

Received 8 January 2010; accepted revised manuscript 22 February 2010.
Published online 8 March 2010 in Wiley InterScience (www.interscience.wiley.com). DOI 10.1002/humu.21235

ABSTRACT: Autosomal recessive hypotrichosis (ARH) is characterized by sparse hair on the scalp without other abnormalities. Three genes, *DSG4*, *LIPH*, and *LPAR6* (*P2RY5*), have been reported to underlie ARH. We performed a mutation search for the three candidate genes in five independent Japanese ARH families and identified two *LIPH* mutations: c.736T>A (p.Cys246Ser) in all five families, and c.742C>A (p.His248Asn) in four of the five families. Out of 200 unrelated control alleles, we detected c.736T>A in three alleles and c.742C>A in one allele. Haplotype analysis revealed each of the two mutant alleles is derived from a respective founder. These results suggest the *LIPH* mutations are prevalent founder mutations for ARH in the Japanese population. *LIPH* encodes PA-PLA$_1\alpha$ (LIPH), a membrane-associated phosphatidic acid-preferring phospholipase A$_1\alpha$. Two residues, altered by these mutations, are conserved among PA-PLA$_1\alpha$ of diverse species. Cys^{246} forms intramolecular disulfide bonds on the lid domain, a crucial structure for substrate recognition, and His^{248} is one amino acid of the catalytic triad. Both p.Cys246Ser- and p.His248Asn-PA-PLA$_1\alpha$ mutants showed complete abolition of hydrolytic activity and had no P2Y5 activation ability. These results suggest defective activation of P2Y5 due to reduced 2-acyl lysophosphatidic acid production by the mutant PA-PLA$_1\alpha$ is involved in the pathogenesis of ARH.
Hum Mutat 31:602–610, 2010. © 2010 Wiley-Liss, Inc.

KEY WORDS: LIPH; Lysophosphatidic Acid; Phosphatidic Acid; Lid Domain; Catalytic Triad; LAH2; LAH

Introduction

Autosomal recessive hypotrichosis (ARH; MIM#s 607892, 607903, 611452) is a rare form of alopecia characterized by sparse hair on the scalp, sparse to absent eyebrows and eyelashes, and sparse axillary and body hair. Wali et al. [2007] noted clinical similarities among three genetically distinct forms of hypotrichosis, localized autosomal recessive hypotrichosis (LAH), and proposed that the forms mapped to chromosome 18q12.1, 3q27.2, and 13q14.11–q21.32 are designated as LAH1, LAH2, and LAH3, respectively. Recently, causative genes for all three forms were identified. Mutations in the desmoglein-4 gene (*DSG4*; MIM# 607892) lead to LAH1 [Kljuic et al., 2003; Rafique et al., 2003]. Mutations in *LIPH* (MIM# 607365), which encodes membrane-associated phosphatidic acid-preferring phospholipase A$_1\alpha$ (PA-PLA$_1\alpha$[LIPH]), underlie LAH2 [Ali et al., 2007; Kazantseva et al., 2006]. Most recently, Pasternack et al. [2008] and Shimomura et al. [2008] reported that mutations in the lysophosphatidic acid receptor 6 gene *LPAR6* (*P2RY5*; MIM# 609239) caused LAH3.

In this study, we searched for mutations in the *DSG4*, *LIPH*, and *LPAR6* genes in five unrelated Japanese families with ARH. Surprisingly, we found two prevalent missense mutations in the *LIPH* gene in all of the families. Furthermore, one mutation c.736T>A (p.Cys246Ser) was found in all five families, and the other mutation c.742C>A (p.His248Asn) was detected in four of the five families. We clarified that these two mutations are strong founder mutations in *LIPH* in the Japanese population. In addition, we evaluated the enzyme activity of mutant PA-PLA$_1\alpha$ derived from the two mutant alleles. We also analyzed the abilities of the mutant PA-PLA$_1\alpha$ to activate lysophosphatidic acid receptor 6 (P2Y5), to clarify the pathogenetic pathway of ARH.

Materials and Methods

Subjects

Five unrelated nonconsanguineous Japanese families A, B, C, D, and E (Fig. 1) with ARH were seen in our hospital or referred to us for the past 5 years. Families A, C, and D were from Hokkaido, the northern most major island of Japan. Families B and E were from western and central Japan, respectively. The medical ethics committee of Hokkaido University approved all the described studies. The study was conducted according to the Declaration of Helsinki Principles. The patients gave written informed consent.

*Correspondence to: Masashi Akiyama, Department of Dermatology, Hokkaido University Graduate School of Medicine, North 15 West 7, Sapporo 060-8638, Japan. E-mail: akiyama@med.hokudai.ac.jp

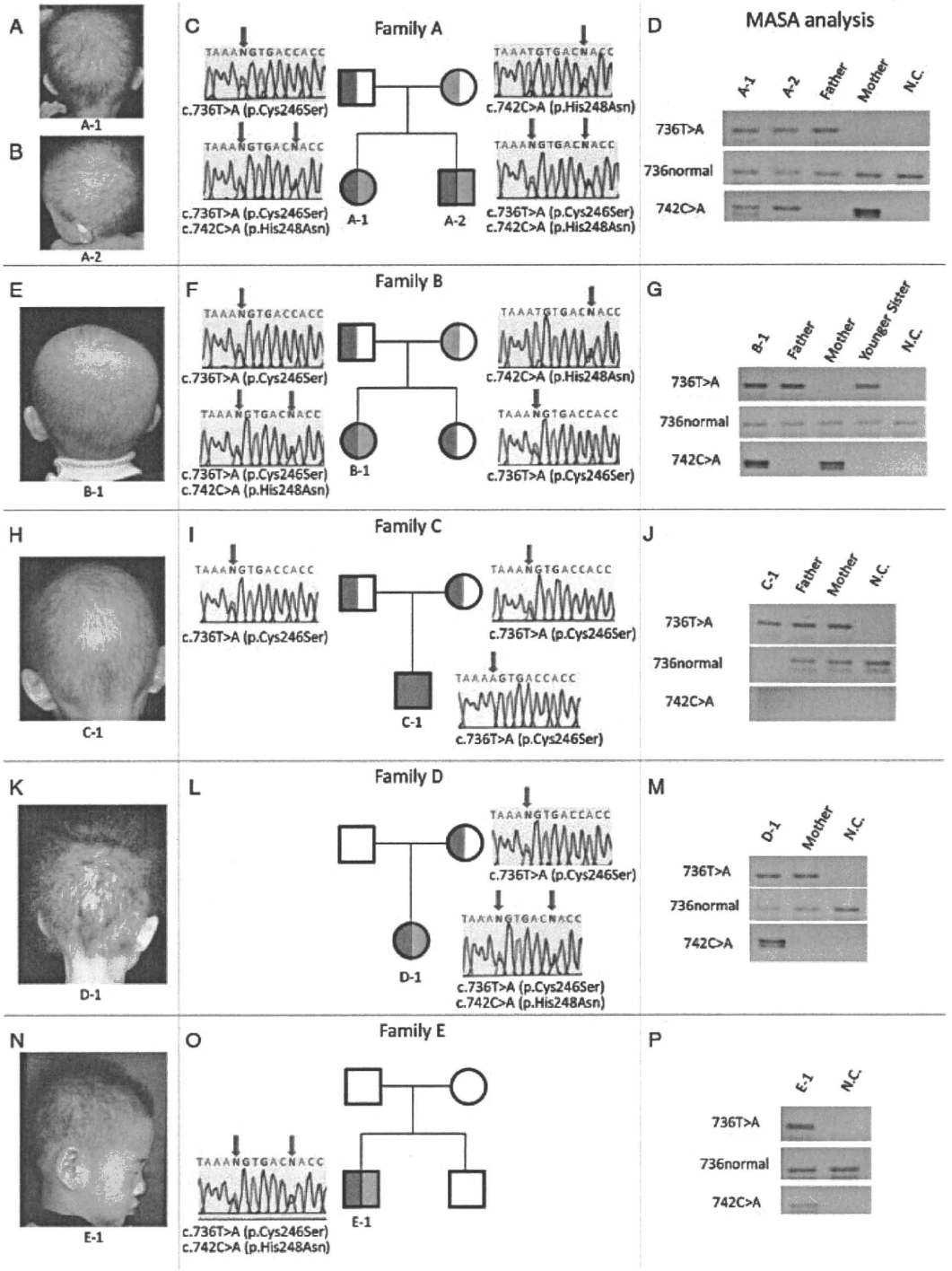

Figure 1. Clinical features of five Japanese families with ARH and identification of mutations in the *LIPH* gene. **A, B, E, H, K, N:** All the affected individuals have features of ARH, which is characterized by sparse hair on the scalp and slightly sparse to absent eyebrows and eyelashes. **C, F, I, L, O:** Pedigrees of the families. Family A (C), Family B (F), Family C (I), Family D (L), and Family E (O) are consistent with autosomal recessive inheritance. Direct sequencing of the *LIPH* gene revealed that patients A-1, A-2, B-1, D-1, and E-1 had compound heterozygous missense mutations involving c.736T>A and c.742C>A, whereas patient C-1 had a homozygous c.736T>A missense mutation. **D, G, J, M, P:** Mutant-allele-specific amplification (MASA) analysis. (Upper) With c.736T>A mutant allele-specific primers, the amplification bands from the c.736T>A mutant alleles are detected by direct sequencing as 301 bp fragments only in the patients and their family members who had the c.736T>A missense mutation, confirming the presence of the mutation. (Middle) With c.736 wild-type allele-specific primers, no PCR product was detected in patient C-1, who was homozygous for c.736T>A. PCR products from the other patients who were compound heterozygous for the two missense mutations c.736T>A and c.742C>A, from unaffected family members and from the normal control (N.C.) were amplified by wild-type allele-specific amplification. (Lower) With c.742C>A mutant-allele-specific primers, the amplification bands from the c.742C>A mutant alleles were detected as 297 bp fragments only in the PCR products from the DNA samples of the patients and their family members who had the c.742C>A missense mutation, confirming the presence of the mutation.

Mutation Detection

DSG4, LIPH, and *LPAR6* mutation search was performed as previously reported [Moss et al., 2004; Pasternack et al., 2008; Shimomura et al., 2008, 2009b]. Briefly, genomic DNA (gDNA) isolated from peripheral blood was subjected to polymerase chain reaction (PCR) amplification, followed by direct automated sequencing using an ABI PRISM 3100 genetic analyzer (Advanced Biotechnologies, Columbia, MD), and verification of the mutations by mutant-allele-specific amplification (MASA) analysis.

Oligonucleotide primers were designed using the Website program (www.bioinformatics.nl/cgi-bin/primer3plus/primer3plus.cgi). The entire coding regions of *DSG4, LIPH,* and *LPAR6,* including the exon/intron boundaries, were sequenced using gDNA samples from patients and their family members, after fully informed consent. For normal controls, 100 healthy unrelated Japanese individuals (200 normal alleles) were studied.

The complementary DNA (cDNA) nucleotides and the amino acids of the protein were numbered based on the previous sequence information (GenBank accession number, *DSG4*; AY177664.1, *LIPH*; AY093498.1, *LPAR6*; AF000546.1) [Jin et al., 2002; Whittock and Bower, 2003]. Nucleotide numbering reflects cDNA numbering with +1 corresponding to the A of the ATG translation initiation codon in the reference sequence, according to journal guidelines (www.hgvs.org/mutnomen). The initiation codon is codon 1.

Mutant Allele-Specific Amplification Analysis

For verification of the mutation, using PCR products as a template, mutant allele specific amplification analysis was performed with mutant allele-specific primers carrying the substitution of a base at the 3′-end [Hasegawa et al., 1995; Xu et al., 2003], as follows: c.736T>A mutant allele-specific forward primer, 5′-CCAAGGATTTCAGTATTTTAAAA-3′; c.736 normal allele-specific forward primer, 5′-CCAAGGATTTCAGTATTTTAAAT-3′; c.742C>A mutant allele-specific forward primer, 5′-GGATTTCAGTATTTTAAATGTGACA-3′; reverse primer, 5′-GTGCCCAGCAGAAAAACAAG-3′.

PCR conditions were as follows: 94°C for 5 min, followed by 35 cycles at 94°C for 1 min, 60°C (for c.736T>A mutant amplification) or 64°C (for c.742C>A mutant amplification) for 1 min, and extension at 72°C for 7 min. Only 301- and 297-bp fragments derived from the mutant alleles were amplified with these primers and the PCR condition, respectively.

Haplotype Analysis

To determine whether the mutations c.736T>A and c.742C>A are founder mutations, we performed haplotype analysis. We constructed linkage disequilibrium (LD) blocks containing the *LIPH* gene using genotype data from the HapMap database (International HapMap Consortium, 2005). The haplotype structure with its tag-single nuclotide polymorphisms (SNPs) was determined using Haploview [Barrett et al., 2005]. We genotyped 10 tag-SNPs using the ABI PRISM 3100 genetic analyzer (Advanced Biotechnologies). Oligonucleotide primers were designed using the website program (www.bioinformatics.nl/cgi-bin/primer3plus/primer3plus.cgi).

Construction of Mutated *LIPH* Gene Expression Vectors

Normal human full-length *LIPH* cDNA was amplified by reverse transcription-PCR using human colon-derived total RNA [Sonoda et al., 2002]. The DNA fragment covering the coding region of PA-PLA$_1\alpha$ (EcoRI–EcoRI fragment) was subcloned into the EcoRI site of pCAGGS mammalian expression vector (kindly donated by Dr. Junichi Miyazaki, Osaka University) [Hiramatsu et al., 2003]. Short *LIPH* fragments (64 bp) (c.695–758) including either the c.736T>A or the c.742C>A mutation were synthesized by IDT Inc. (Coralville, IA). pCAGGS vector including the rest of the *LIPH* gene was amplified with specific primers as follows: forward (5′-CCTGTACCTGTCTTCCCTGAG-3′) and reverse (5′-CAGGTTGATCCAATCCTCCA-3′). PCR was carried out using KOD-Plus-Ver.2 (Toyobo, Osaka, Japan) according to the instructions. Finally, the synthesized mutated DNA fragments were ligated with the amplified pCAGGS vector including the *LIPH* gene without 64 bp oligonucleotide (c.695–758) using a Ligation-Convenience Kit (Nippon Gene Co., Tokyo, Japan).

Expression of Mutated PA-PLA$_1\alpha$ in HEK293 Cells

To investigate the molecular defects underlying the mutations that were identified in this study, we synthesized p.Cys246Ser or p.His248Asn mutations in PA-PLA$_1\alpha$ expression constructs and compared mutant protein expression with wild-type (WT) and p.Ser154Ala PA-PLA$_1\alpha$ protein. Previously, Sonoda et al. [2002] reported that Ser^{154} was the active catalytic residue and that the p.Ser154Ala mutant PA-PLA$_1\alpha$ had complete loss of enzyme activity, although the amount of p.Ser154Ala mutant protein expressed was almost the same as that of WT protein. Thus, we used the p.Ser154Ala mutant as a loss-of-function mutant control in this study.

HEK293 cells were maintained in Dulbecco's modified Eagle's medium supplemented with antibiotics and 10% fetal bovine serum under an atmosphere of 5% CO_2 at 37°C. The resulting cDNAs were used to transfect HEK293 cells using LipofectAMINE 2000 reagent (Invitrogen, Carlsbad, CA) according to the manufacturer's protocol. HEK293 cells were transfected with WT, p.Ser154Ala (control loss-of-function mutant) [Sonoda et al., 2002], p.Cys246Ser or p.His248Asn PA-PLA$_1\alpha$.

Preparation of Cell Supernatants and Lysates and Western Blotting

HEK293 cells transfected with pCAGGS vector were maintained for an additional 24 hr after the medium was changed to serum-free medium ExCell302 (JRH Biosciences, Lenexa, KS). After 24 hr of incubation, the media were collected and precipitated with trichloroacetic acid. Precipitated protein was collected by centrifugation at 15,000 × *g* for 20 min, followed by washing with acetone twice; then, the pellet was redissolved in sodium dodecyl sulfate (SDS) sample buffer A (62.5 mM Tris-HCl [pH 6.8], 10% Glycerol, 2% SDS, 5% 2-mercaptoethanol (2ME), 10 μg/mL phenylmethylsulphonyl fluoride [PMSF]) and boiled for 5 min. HEK293 cells were harvested 48 hr after transfection and SDS sample buffer B (62.5 mM Tris-HCl [pH 6.8], 4 M Urea, 10% Glycerol, 2% SDS, 5% 2ME, 10 μg/mL PMSF) was added directly to the cell pellet. The pellet was then sonicated and boiled for 5 min.

These protein samples of cell supernatants and lysates were separated by SDS-polyacrylamide gel electrophoresis (SDS-PAGE) and transferred to nitrocellulose membrane. The nitrocellulose membrane was blocked with Tris-buffered saline containing 5% (w/v) skimmed milk and 0.05% (v/v) Tween 20, incubated with anti-PA-PLA$_1\alpha$ monoclonal antibody [Sonoda et al., 2002], and then treated with antirat IgG antibody conjugated with horseradish peroxidase. Proteins bound to the antibodies were

visualized with an enhanced chemiluminescence kit (ECL, Amersham Biosciences, Piscataway, NJ) by LAS4000 Luminescent Image Analyzer (Fujifilm, Tokyo, Japan) [Sonoda et al., 2002].

PA-PLA$_1\alpha$ Enzyme Activity Assay

PA-PLA$_1\alpha$ produces 2-acyl lysophosphatidic acid (LPA) and free fatty acid (FFA) concurrently from phosphatidic acid (PA) [Sonoda et al., 2002]. In the present study, the hydrolysis activity was determined measuring oleic acids, which are concurrently produced from dioleoyl PA by PA-PLA$_1\alpha$. We added the supernatant from HEK293 cells transfected with WT, p.Ser154Ala, p.Cys246Ser, or p.His248Asn PA-PLA$_1\alpha$ to the medium including 100 μM PA. After 12 hr incubation at 37°C, the amount of oleic acids was measured with NEFA C-Test Wako test kit (Wako Chemicals Co., Osaka, Japan).

P2Y5 Activation Ability Assay

We cotransfected alkaline-phosphatase-tagged transforming growth factor-α (AP-TGFα) (kindly provided by Dr. Higashiyama, Ehime University, Japan) [Tokumaru et al., 2000], recombinant P2Y5 and WT, p.Ser154Ala, p.Cys246Ser, or p.His248Asn PA-PLA$_1\alpha$ to HEK293 cells, and we quantified free AP-TGFα induced by a disintegrin and metalloprotease (ADAM) in the HEK293 cells to examine the P2Y5 activation ability of LPA produced by mutant PA-PLA$_1\alpha$. Cells were cultured in 100 μL of serum-free medium Opti-MEM (Gibco BRL, Grand Island, NY) in individual wells of a 96-well plate. After 24 hr of incubation, 80 μL of the conditioned medium in each well was transferred and AP activities in both the conditioned media and the transfected cells were measured using *p*-nitrophenyl phosphate (*p*-NPP). In the case of phorbol ester, 12-O-tetradecanoylphorbol-13-acetate (TPA)-stimulation, the transfected cells were treated with 100 nM 1 h before medium transfer. The AP reaction was performed in *p*-NPP buffer (5 mM *p*-NPP, 20 mM Tris-HCl (pH 9.5), 20 mM NaCl, and 5 mM $MgCl_2$) at 37°C for 1 hr and the increases in the reaction product, *p*-nitrophenol, were quantified by monitoring absorbance at 405 nm with VersaMax microplate reader (Molecular Devices, Sunnyvale, CA). The amount of AP-TGFα released was expressed as a ratio of AP activity in the conditioned media to total AP activity in each well.

Results

Clinical Findings

All six affected individuals in the five unrelated Japanese families showed features typical of ARH (Fig. 1A, B, E, H, K, and N). The patients were less than 10 years of age at the time of the study. Affected individuals had tightly curled hair, which grew slowly and stopped growing after a few inches. Their eyebrows and eyelashes were a little sparse to absent. Nails, teeth, sweating, and hearing were normal in all the affected individuals. Heterozygous carriers had normal hair. The pedigrees of all the families were consistent with autosomal recessive inheritance (Fig. 1C, F, I, L, and O).

Mutation Detection

Direct sequencing analysis of exons and intron–exon boundaries of *LIPH* revealed that affected members of Families A, B, D, and E were compound heterozygous for the two missense mutations c.736T>A (p.Cys246Ser) and c.742C>A (p.His248Asn) (Fig. 1C, F, I, L, O). The affected individual in Family C was homozygous for c.736T>A. All the parents whose DNA was available for mutation search were heterozygous carriers of one of the two mutations (Fig. 1C, F, I, L, and O). We confirmed these *LIPH* mutations by MASA analysis (Fig. 1D, G, J, M, and P). Both amino acid residues altered by the two missense mutations were highly conserved among diverse species (Fig. 2A). One of the mutations was found in 4/200 normal unrelated alleles (100 healthy Japanese individuals) by direct sequence analysis (minor allele frequency, c.736T>A, 0.015 (3/200); c. 742C>A, 0.005 (1/200); combined genotype 0.02 (4/200)), although there was no control individual who had compound heterozygous or homozygous mutations (data not shown). No other pathogenic mutation was found in the entire exon or intron/exon borders of the *DSG4*, *LIPH* or *LPAR6* gene.

Haplotype Aanalysis

The haplotype block structure containing the *LIPH* gene was constructed using genotype data from the HapMap database (Fig. 3B). The haplotype block was represented by five haplotypes with >1% frequency (Fig. 3C). The haplotype of the chromosome containing the *LIPH* c.736T>A mutation was found to have resulted from parent-to-child transmission in all five families (Table 1). The chromosome containing the *LIPH* c.736T>A mutation had haplotype I (ATCAACCGGA), which is seen in 37.8% of the Han Chinese and ethnic Japanese populations. Likewise, we determined the haplotype of the chromosome containing the *LIPH* c.742C>A mutation in four families (A, B, D, E). The chromosome containing the *LIPH* c.742C>A mutation had haplotype III (GCTCGTGAGG), which is seen in 28.9%. Thus, these missense mutations c.736T>A (p.Cys246Ser) and c.742C>A (p.His248Asn) in Japanese patients appear to represent founder effects in this island nation.

Expression of PA-PLA$_1\alpha$ in Mammalian Cells

Immunoblot analysis revealed that transfection of p.Cys246Ser and p.His248Asn mutant constructs into HEK293 cells resulted in the secretion of 55-kDa mutant PA-PLA$_1\alpha$ at a level similar to that of the WT and of the p.Ser154Ala mutant (Fig. 4A). In addition, the same amounts of mutant PA-PLA$_1\alpha$ proteins were also recovered from the cell lysate. These results indicated that there was no significant difference in protein yield between WT and mutant PA-PLA$_1\alpha$.

Analysis of PA-PLA$_1\alpha$ Hydrolytic Activity

The hydrolysis activity was determined measuring FFA which are concurrently produced from PA by PA-PLA$_1\alpha$. The quantities of FFA produced by the p.Cys246Ser and p.His248Asn mutant *LIPH* constructs were similar to those by the mock and p.Ser154Ala mutant constructs, suggesting that the p.Cys246Ser and p.His248Asn mutant PA-PLA$_1\alpha$ had no hydrolytic activity (Fig. 4B).

P2Y5 Activation Ability of PA-PLA$_1\alpha$ Mutants

In this study, we cotransfected AP-TGFα, recombinant P2Y5 and WT, p.Ser154Ala, p.Cys246Ser, or p.His248Asn PA-PLA$_1\alpha$ constructs to HEK293 cells. To examine the P2Y5 activation potency of mutant PA-PLA$_1\alpha$, AP-TGFα release into conditioned media via ADAM, which was triggered by activation of P2Y5, was

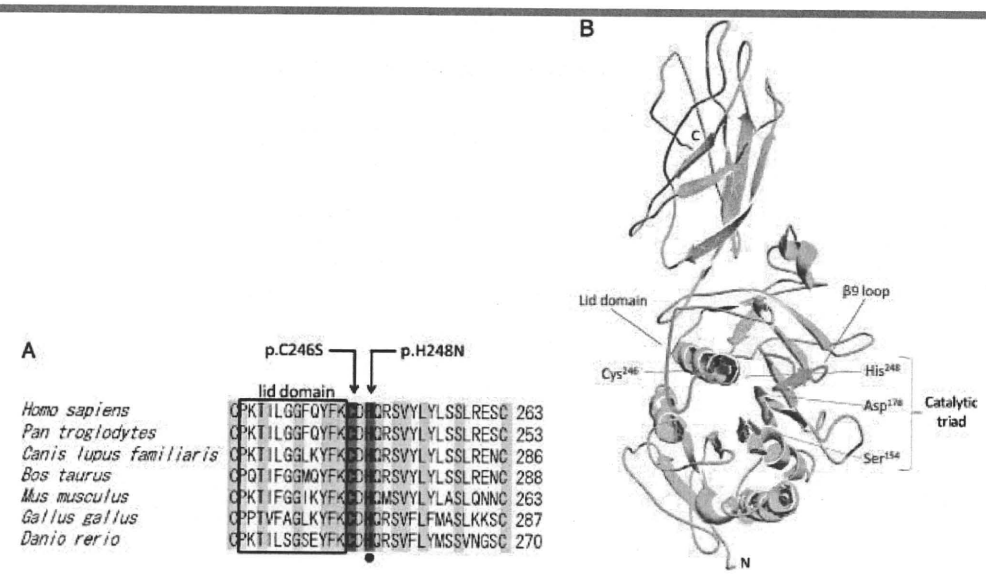

Figure 2. Conservation of the mutated residues and the three-dimensional protein structure around the mutation sites. **A**: Multiple amino acid sequence alignments of PA-PLA$_1\alpha$ of diverse species. Amino acid residues Cys^{246} and His^{248} altered by the present two mutations are highly conserved among PA-PLA$_1\alpha$ of diverse species. Amino acid residues that are conserved between the seven species are shown in yellow. The 12 residues that comprise the lid domain are surrounded by a black rectangle. One of the amino acids of the catalytic triad, His^{248}, is marked with a black dot. Cys^{246} and His^{248} are in red and indicated by arrows. **B**: The three-dimensional-structure model of PA-PLA$_1\alpha$ protein. Cys^{246} and His^{248} residues are in red. Lid domain and β9loop are in green. Catalytic triad consists of Ser^{154} (purple), Asp^{178} (purple) and His^{248}. Cys^{246} forms intramolecular disulfide bonds on the lid domain.

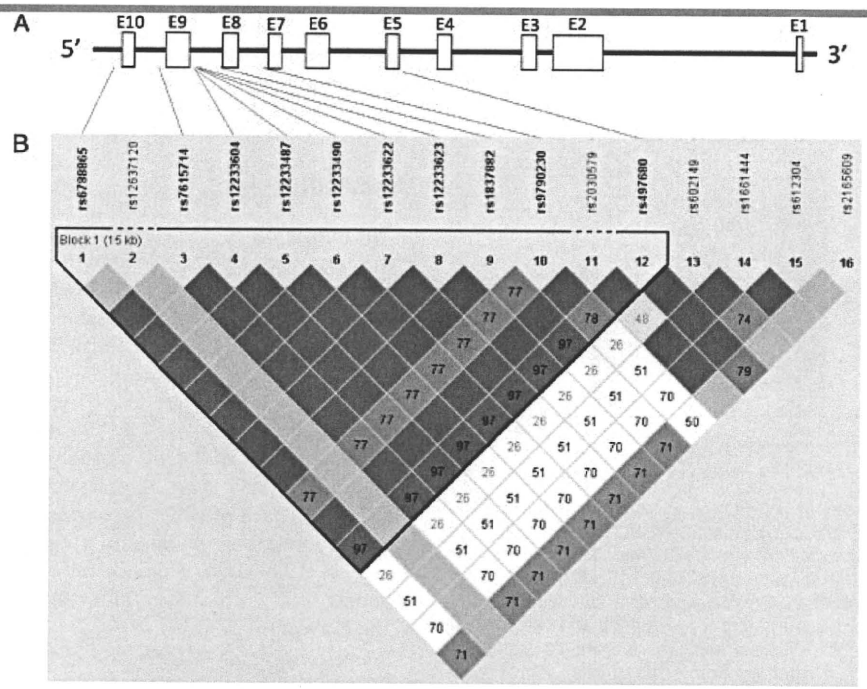

Figure 3. The linkage disequilibrium (LD) block and the haplotype structure around *LIPH* in Han Chinese and ethnic Japanese populations. *LIPH* structure (**A**) and the LD block within *LIPH* (**B**) were evaluated using genotype data from the HapMap database. **C**: The haplotype structure with 10 tag-SNPs was determined using Haploview.

Table 1. Identified Haplotype with the *LIPH* c.736T>A and c.742C>A Mutation

Family	Mutation	rs6788865	rs7615714	rs12233604	rs12233487	rs12233490	rs12233622	rs12233623	rs1837882	rs9790230	rs497680	Haplotype
A	c.736T>A	A/G	T/C	C/T	A/C	A/G	C/T	C/G	G/A	G/G	A/G	I/III
	c.742C>A	A/G	T/C	C/T	A/C	A/G	C/T	C/G	G/A	G/G	A/G	I/III
B	c.736T>A	A	T	C	A	A	C	C	G	G	A	I
	c.742C>A	G	C	T	C	G	T	G	A	G	G	III
C (homozygote)	c.736T>A	A	T	C	A	A	C	C	G	G	A	I
D	c.736T>A	A	T	C	A	A	C	C	G	G	A	I
	c.742C>A	G	C	T	C	G	T	G	A	G	G	III
E	c.736T>A	A/G	T/C	C/T	A/C	A/G	C/T	C/G	G/A	G/G	A/G	I/III
	c.742C>A	A/G	T/C	C/T	A/C	A/G	C/T	C/G	G/A	G/G	A/G	I/III

Nucleotide numbering starts at +1 corresponding to the A of the ATG initiation codon in the reference sequence AY093498.1 (www.hgvs.org/mutnomen). SNP, single-nucleotide polymorphism.

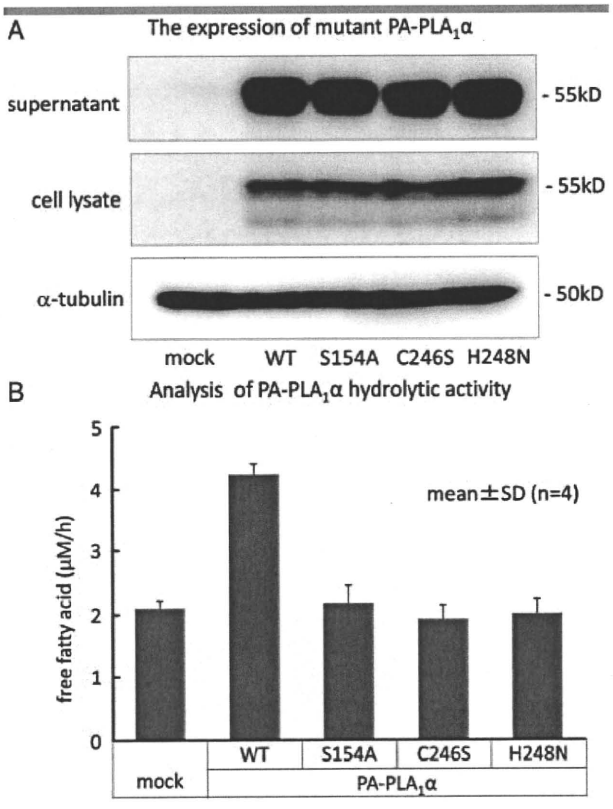

Figure 4. Expression of PA-PLA$_1\alpha$ in HEK293 cells and its hydrolytic activity. **A:** Expression of mutant PA-PLA$_1\alpha$ in HEK293 cells. HEK293 cells were transfected with wild-type (WT), p.Ser154Ala (S154A), p.Cys246Ser (C246S), and p.His248Asn (H248N) *LIPH* cDNA, and the expression level of PA-PLA$_1\alpha$ protein derived from the constructs in cell culture supernatant (upper panel) and cells (middle panel) were evaluated by Western blot. There were no significant differences in PA-PLA$_1\alpha$ protein expression levels among cells trasfected with WT, S154A, C246S, and H248N. α-tubulin expression was used as a standard to assess the total amount of proteins from cell lysate loaded on the gel (lower panel). **B:** Because PA-PLA$_1\alpha$ hydrolyzes the free fatty acid (FFA) from PA, we monitored the levels FFA to determine whether there is a difference in the PA-PLA$_1\alpha$ hydrolytic activity among WT and the three mutants of PA-PLA$_1\alpha$. After 12-hr incubation of the supernatant from HEK293 cells expressing WT, S154A, C246S, or H248N PA-PLA$_1\alpha$, with a medium including 100 μM PA, the levels of FFA hydrolyzed by C246S and H248N mutant PA-PLA$_1\alpha$ were significantly lower than that by WT PA-PLA$_1\alpha$ and similar to those produced by supernatant from HEK293 cells transfected with control S154A mutant and an empty vector (mock).

quantified using *p*-NPP as a substrate for AP. The free AP-TGFα from the P2Y5 mock transfected (P2Y5-) cells transfected with the WT form of PA-PLA$_1\alpha$ was more abundant than that from the P2Y5− cells transfected with empty vector, which indicated that the HEK293 cells had the ability to shed TGFα mediated by intrinsic LPA receptor at some level (Fig. 5A). AP-TGFα release from P2Y5 positive (P2Y5+) cells expressing the WT PA-PLA$_1\alpha$ was remarkably increased compared with mock or mutant PA-PLA$_1\alpha$. There were no significant differences between the data obtained with cells expressing the mutants and the empty vector (Fig. 5A). All the cells expressing AP-TGFα responded equally to TPA, confirming that expression of P2Y5 and PA-PLA$_1\alpha$ did not affect PKC-dependent AP-TGFα release (Fig. 5B). These data clearly indicated that these mutations resulted in the loss of P2Y5 activation activity of PA-PLA$_1\alpha$.

Discussion

The human *LIPH* gene encodes PA-PLA$_1\alpha$, which is a member of the membrane-associated phosphatidic acid-preferring phospholipase A$_1\alpha$ [Hiramatsu et al., 2003; Jin et al., 2002; Sonoda et al., 2002]. Similar to other phospholipase A$_1$, PA-PLA$_1\alpha$ has N-terminal domains that are essential for catalytic activity. Three amino acid residues, Ser^{154}, Asp^{178}, and His^{248}, which form the putative catalytic triad, are located in the N-terminal domains [Aoki et al., 2007; Jin et al., 2002; Kubiak et al., 2001; Sonoda et al., 2002] (Fig. 2B). PA-PLA$_1\alpha$ has a β9 loop (the 13 amino acids from p.206 to 218) and a short lid domain (the 12 amino acids from p.234 to245), each of which is considered a crucial structure for substrate recognition [Aoki et al., 2007; Carriere et al., 1998; Sonoda et al., 2002]. In addition, well-conserved cysteine residues including Cys^{246}, which form intramolecular disulfide bonds, are in the N-terminal domains.

We performed *DSG4*, *LIPH*, and *LPAR6* gene mutation analysis and identified two prevalent missense mutations in the *LIPH* gene in the five independent Japanese ARH families. One mutation c.736T>A leads to an amino acid change within conserved cysteine residue that forms intramolecular disulfide bonds on the lid domain (p.Cys246Ser) (Fig. 2). The other mutation c.742C>A results in alteration of one amino acid of the catalytic triad (p.His248Asn) (Fig. 2B). These two residues, Cys^{246} and His^{248}, are highly conserved among *LIPH* of diverse species (Fig. 2A), suggesting that they play a critical role in enzyme activity. We speculate that these mutations drastically affect PA-PLA$_1\alpha$ activity.

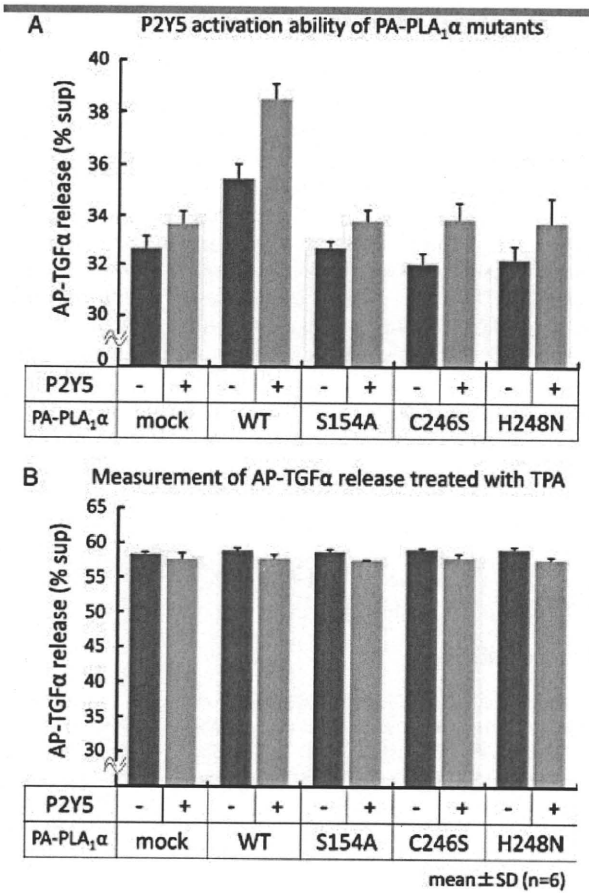

Figure 5. P2Y5 activation ability of PA-PLA$_1$α mutants. To monitor P2Y5 activation level by mutant and wild-type (WT) PA-PLA$_1$α, we used *p*-nitrophenyl phosphate as a substrate for cleavage of AP-TGFα and measured the amount of AP-TGFα released from the HEK293 cells. **A:** The amount of free AP-TGFα produced by P2Y5 mock-transfected (P2Y5−) cells that were also transfected with WT PA-PLA$_1$α is significantly greater than that produced by P2Y5− cells transfected with an empty vector (mock). This indicates that HEK293 cells act to shed AP-TGFα, an activity that might be mediated by intrinsic LPA receptors. The amounts of AP-TGFα released from P2Y5-transfected (P2Y5+) cells expressing p.Ser154Ala (S154A), p.Cys246-Ser (C246S), or p.His248Asn (H248N) mutant PA-PLA$_1$α and P2Y5+ cells transfected with an empty vector (mock) are significantly lower than that from P2Y5+ cells expressing WT PA-PLA$_1$α. **B:** TPA sheds AP-TGFα independently from the P2Y5 pathway. Effects of the TPA-induced shedding of AP-TGFα are similar in all the cells.

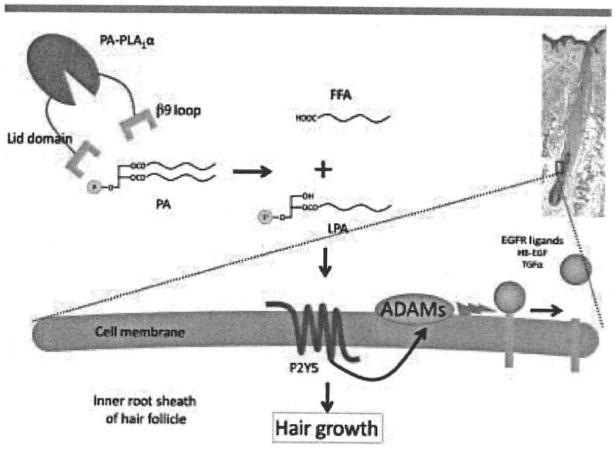

Figure 6. Schematic signaling pathways of LPA produced by PA-PLA$_1$α via the P2Y5 receptor. PA-PLA$_1$α hydrolyzes PA and produces LPA and FFA. LPA works as a ligand for P2Y5, a membrane-bound G-protein-coupled receptor. It has been documented that ADAM activation by P2Y5 results in ectodomain shedding of cell surface proteins including those of the EGF ligand family, such as HB-EGF and TGFα. These signal pathways are speculated to regulate proliferation and differentiation of inner root sheath cells of hair follicles. Abbreviations: PA, phosphatidic acid; FFA, free fatty acid; LPA, 2-acyl lysophosphatidic acid; ADAM, a disintegrin and metalloprotease; EGF, epidermal growth factor; HB-EGF, heparin binding EGF-like growth factor; TGFα, transforming growth factor-α.

So far, 14 *LIPH* gene mutations have been reported, four of which are prevalent [Ali et al., 2007; Horev et al., 2009; Jelani et al., 2008; Kamran-ul-Hassan Naqvi et al., 2009; Kazantseva et al., 2006; Nahum et al., 2009; Naz et al., 2009; Pasternack et al., 2009; Petukhova et al., 2009; Shimomura et al., 2009a,b,c]. One prevalent mutation, 985-bp deletion including exon 4 and the flanking introns, was detected in a large number of ARH patients from two ethnic groups, the Chuvash and Mari, in the Volga–Ural region of Russia [Kazantseva et al., 2006]. The ancestors of the Chuvash population settled in territory occupied by ancestral Mari populations. To determine the frequency of the mutant allele, they tested 2,292 chromosomes in the populations and found the *LIPH* deletion in populations of Chuvash (mutant allele frequency $P = 0.033$) and Mari (mutant allele frequency $P = 0.030$) origin. The mutant allele was restricted to these two populations and was not found in other Finno–Ugric populations or Russian populations from distant geographic regions [Kazantseva et al., 2006].

A deletion mutation exon7_8del has been identified in five consanguineous Pakistani families and 1 Guyanese family [Jelani et al., 2008; Petukhova et al., 2009; Shimomura et al., 2009b, 2009c]. A small deletion mutation 659_660delTA has been identified in several consanguineous Pakistani families and 1 Guyanese family [Jelani et al., 2008; Petukhova et al., 2009; Shimomura et al., 2009b,c]. Both mutations were defined as founder mutations shared in families from Pakistan and Guyana by haplotype analysis using microsatellite markers close to the *LIPH* gene [Jelani et al., 2008; Petukhova et al., 2009; Shimomura et al., 2009b,c]. In fact, these Guyanese families with ARH were descended from people who had come from India about 100 years ago, and it is plausible that both mutations originated from the Indian population [Shimomura et al., 2009c]. However, neither exon7_8del nor 659_660delTA mutations were detected in healthy control individuals of Pakistani origin and their minor allele frequencies were thought to be low in the Pakistani population [Jelani et al., 2008; Shimomura et al., 2009b].

All six of the Japanese ARH patients from the five families in the present study were compound heterozygous for c.736T>A (p.Cys246Ser) and c.742C>A (p.His248Asn) or homozygous for c.736T>A (p.Cys246Ser). c.736T>A (p.Cys246Ser) was found in all five families, and c.742C>A (p.His248Asn) was detected in four of the five families. Most recently, these missense mutations were identified in three Japanese ARH families [Shimomura et al., 2009a]. One family carries two heterozygous missense mutations, c.736T>A and c.742C>A, and the other two families are homozygous for the mutation c.736T>A. Thus, the missense mutations c.736T>A (p.Cys246Ser) and c.742C>A (p.His248Asn) are both suggested to be highly prevalent *LIPH* mutations in the Japanese population. In the previous article, however, screening assays with restriction enzymes excluded the existence of both

mutations in 100 unrelated healthy control individuals (200 alleles) of Japanese origin [Shimomura et al., 2009a]. In this study, in contrast, we used direct sequences and MASA analysis and identified these mutations in four alleles out of 200 unrelated control alleles (100 individuals) (minor allele frequency of c.736T>A, 3/200 $P = 0.015$; c. 742C>A, 1/200 $P = 0.005$; combined genotype, 4/200 $P = 0.020$). In addition, the present haplotype analysis revealed that the mutant alleles with c.736T>A and those with c.742C>A had specific haplotypes, respectively, which suggests that they derive from their own independent founders (Fig. 3, Table 1). From these results, we consider that the *LIPH* mutations c.736T>A (p.Cys246Ser) and c.742C>A (p.His248Asn) are extremely prevalent founder mutations for ARH in the Japanese population.

Previously, several deletion mutations and four missense mutations were reported in the *LIPH* gene [Ali et al., 2007; Horev et al., 2009; Jelani et al., 2008; Kamran-ul-Hassan Naqvi et al., 2009; Kazantseva et al., 2006; Nahum et al., 2009; Naz et al., 2009; Pasternack et al., 2009; Petukhova et al., 2009; Shimomura et al., 2009a,b,c]. In previous cases, ARH patients exhibited wide variability in the hypotrichosis phenotype, although most patients showed wooly hair during early childhood [Shimomura et al., 2009b]. Even ARH patients with identical *LIPH* gene mutations showed a wide variation in phenotype [Shimomura et al., 2009b]. In our cases, all the affected individuals had sparse, curled hair that grew slowly from birth and then stopped growing after reaching a few inches. There are no significant differences in clinical features between families and patients. We cannot exclude the possibility that differences in phenotype will emerge in the future, because our patients were still less than 10 years of age. The clinical features of the five families presented here are similar to those of families with the other mutations in the *LIPH* gene, and no apparent genotype/phenotype correlation was observed between the patients with deletion mutations and those with missense mutations.

PA-PLA$_1\alpha$ hydrolyzes PA and produces LPA and FFA concurrently [Sonoda et al., 2002]. The LPA that is produced by PA-PLA$_1\alpha$ acts as a ligand for P2Y5, one of the G-protein-coupled receptors (GPCRs), which has been identified as another causative gene for human hair growth deficiency [Pasternack et al., 2008; Shimomura et al., 2008]. It has been documented that ADAM activation by GPCRs introduces the ectodomain shedding of cell surface proteins, including the epidermal growth factor (EGF) ligand family whose members include heparin-binding EGF-like growth factor (HB-EGF) and TGFα [Ohtsu et al., 2006] (Fig. 6).

In this study, we performed two different in vitro PA-PLA$_1\alpha$ enzyme activity analyses. One involved analyzing PA-PLA$_1\alpha$ hydrolytic activity by measuring FFA (unpublished data). The p.Cys246Ser and p.His248Asn mutants showed complete abolition of PA-PLA$_1\alpha$ hydrolytic activity, comparable with supernatant of cells transfected with the empty vector only or with the control loss-of-function mutant carrying p.Ser154Ala. The other involved analyzing the P2Y5 activation ability of LPA produced by PA-PLA$_1\alpha$ by assaying free AP-TGFα (unpublished data). In this analysis, the p.Cys246Ser and p.His248Asn mutant PA-PLA$_1\alpha$ had no ability to activate P2Y5. These results clearly indicated that a loss of PA-PLA$_1\alpha$ function leads to defective activation of P2Y5 by LPA, resulting in ARH phenotype in ARH patients with *LIPH* mutations. Thus, complete loss of P2Y5 activation due to reduced LPA is thought to be involved in the pathogenesis of ARH.

While we were preparing the manuscript, Pasternack et al. [2009] reported that PA-PLA$_1\alpha$ derived from mutants with c.403_409 duplication frameshift mutation and in-frame mutations including c.280_369dup and c.527_628del did not show the enzymatic activity of converting PA to LPA in vitro, and that they did not activate P2Y5. The results presented in this study completely agree with their results, although the assay system for enzymatic evaluation and P2Y5 activation used by Pasternack et al. [2009] is quite different from ours. In addition, the affected amino acids in the mutant PA-PLA$_1\alpha$ analyzed in this study were quite different. Interestingly, our in vitro enzyme activity analysis revealed that the present two missense mutations strikingly affected the PA-PLA$_1\alpha$ activity as much as frameshift mutations and large deletion mutations like c.403_409 dup, c.280_369dup, and c.527_628del. These results were consistent with the fact that there is no significant difference in severity of hair loss between the present patients with missense mutations and affected individuals with frameshift mutations or large deletion mutations, c.403_409 dup, c.280_369dup, and c.527_628del. These results clearly indicated that the loss of PA-PLA$_1\alpha$ function caused by the two present mutations leads to defective activation of P2Y5 by LPA and suggest that loss of P2Y5 activation due to reduced LPA is involved in the pathogenesis of ARH.

Acknowledgments

We thank the patients for their generous cooperation and Ms. Akari Nagasaki, Ai Hayakawa, Yuko Hayakawa, and Shizuka Miyakoshi for their technical assistance on this project. This work was supported in part by Grant-in-Aid from the Ministry of Education, Science, Sports, and Culture of Japan to M. Akiyama (Kiban B 20390304) and by a grant from Ministry of Health, Labor and Welfare of Japan (Health and Labor Sciences Research Grants; Research on Intractable Diseases; H21-047) to M. Akiyama.

References

Ali G, Chishti MS, Raza SI, John P, Ahmad W. 2007. A mutation in the lipase H (LIPH) gene underlie autosomal recessive hypotrichosis. Hum Genet 121: 319–325.

Aoki J, Inoue A, Makide K, Saiki N, Arai H. 2007. Structure and function of extracellular phospholipase A1 belonging to the pancreatic lipase gene family. Biochimie 89:197–204.

Barrett JC, Fry B, Maller J, Daly MJ. 2005. Haploview: analysis and visualization of LD and haplotype maps. Bioinformatics 21:263–265.

Carriere F, Withers-Martinez C, van Tilbeurgh H, Roussel A, Cambillau C, Verger R. 1998. Structural basis for the substrate selectivity of pancreatic lipases and some related proteins. Biochim Biophys Acta 1376:417–432.

Hasegawa Y, Takeda S, Ichii S, Koizumi K, Maruyama M, Fujii A, Ohta H, Nakajima T, Okuda M, Baba S, Nakamura Y. 1995. Detection of K-ras mutations in DNAs isolated from feces of patients with colorectal tumors by mutant-allele-specific amplification (MASA). Oncogene 10:1441–1445.

Hiramatsu T, Sonoda H, Takanezawa Y, Morikawa R, Ishida M, Kasahara K, Sanai Y, Taguchi R, Aoki J, Arai H. 2003. Biochemical and molecular characterization of two phosphatidic acid-selective phospholipase A1s, mPA-PLA1alpha and mPA-PLA1beta. J Biol Chem 278:49438–49447.

Horev L, Tosti A, Rosen I, Hershko K, Vincenzi C, Nanova K, Mali A, Potikha T, Zlotogorski A. 2009. Mutations in lipase H cause autosomal recessive hypotrichosis simplex with woolly hair. J Am Acad Dermatol 61:813–818.

Jelani M, Wasif N, Ali G, Chishti M, Ahmad W. 2008. A novel deletion mutation in LIPH gene causes autosomal recessive hypotrichosis (LAH2). Clin Genet 74:184–188.

Jin W, Broedl UC, Monajemi H, Glick JM, Rader DJ. 2002. Lipase H, a new member of the triglyceride lipase family synthesized by the intestine. Genomics 80:268–273.

Kamran-ul-Hassan Naqvi S, Raza SI, Naveed AK, John P, Ahmad W. 2009. A novel deletion mutation in the phospholipase H (LIPH) gene in a consanguineous Pakistani family with autosomal recessive hypotrichosis (LAH2). Br J Dermatol 160:194–196.

Kazantseva A, Goltsov A, Zinchenko R, Grigorenko AP, Abrukova AV, Moliaka YK, Kirillov AG, Guo Z, Lyle S, Ginter EK, Rogaev EI. 2006. Human hair growth

deficiency is linked to a genetic defect in the phospholipase gene LIPH. Science 314:982–985.

Kljuic A, Bazzi H, Sundberg JP, Martinez-Mir A, O'Shaughnessy R, Mahoney MG, Levy M, Montagutelli X, Ahmad W, Aita VM, Gordon D, Uitto J, Whiting D, Ott J, Fischer S, Gilliam TC, Jahoda CA, Morris RJ, Panteleyev AA, Nguyen VT, Christiano AM. 2003. Desmoglein 4 in hair follicle differentiation and epidermal adhesion: evidence from inherited hypotrichosis and acquired pemphigus vulgaris. Cell 113:249–260.

Kubiak RJ, Yue X, Hondal RJ, Mihai C, Tsai MD, Bruzik KS. 2001. Involvement of the Arg-Asp-His catalytic triad in enzymatic cleavage of the phosphodiester bond. Biochemistry 40:5422–5432.

Moss C, Martinez-Mir A, Lam H, Tadin-Strapps M, Kljuic A, Christiano AM. 2004. A recurrent intragenic deletion in the desmoglein 4 gene underlies localized autosomal recessive hypotrichosis. J Invest Dermatol 123:607–610.

Nahum S, Pasternack SM, Pforr J, Indelman M, Wollnik B, Bergman R, Nothen MM, Konig A, Khamaysi Z, Betz RC, Sprecher E. 2009. A large duplication in LIPH underlies autosomal recessive hypotrichosis simplex in four Middle Eastern families. Arch Dermatol Res 301:391–393.

Naz G, Khan B, Ali G, Azeem Z, Wali A, Ansar M, Ahmad W. 2009. Novel missense mutations in lipase H (LIPH) gene causing autosomal recessive hypotrichosis (LAH2). J Dermatol Sci 54:12–16.

Ohtsu H, Dempsey PJ, Eguchi S. 2006. ADAMs as mediators of EGF receptor transactivation by G protein-coupled receptors. Am J Physiol Cell Physiol 291:C1–C10.

Pasternack SM, von Kugelgen I, Aboud KA, Lee YA, Ruschendorf F, Voss K, Hillmer AM, Molderings GJ, Franz T, Ramirez A, Nürnberg P, Nöthen MM, Betz RC. 2008. G protein-coupled receptor P2Y5 and its ligand LPA are involved in maintenance of human hair growth. Nat Genet 40:329–334.

Pasternack SM, von Kugelgen I, Muller M, Oji V, Traupe H, Sprecher E, Nothen MM, Janecke AR, Betz RC. 2009. In vitro analysis of LIPH mutations causing hypotrichosis simplex: evidence confirming the role of lipase H and lysophosphatidic acid in hair growth. J Invest Dermatol 129:2772–2776.

Petukhova L, Shimomura Y, Wajid M, Gorroochurn P, Hodge SE, Christiano AM. 2009. The effect of inbreeding on the distribution of compound heterozygotes: a lesson from Lipase H mutations in autosomal recessive woolly hair/hypotrichosis. Hum Hered 68:117–130.

Rafique MA, Ansar M, Jamal SM, Malik S, Sohail M, Faiyaz-Ul-Haque M, Haque S, Leal SM, Ahmad W. 2003. A locus for hereditary hypotrichosis localized to human chromosome 18q21.1. Eur J Hum Genet 11: 623–628.

Shimomura Y, Ito M, Christiano AM. 2009a. Mutations in the LIPH gene in three Japanese families with autosomal recessive woolly hair/hypotrichosis. J Dermatol Sci 56:205–207.

Shimomura Y, Wajid M, Ishii Y, Shapiro L, Petukhova L, Gordon D, Christiano AM. 2008. Disruption of P2RY5, an orphan G protein-coupled receptor, underlies autosomal recessive woolly hair. Nat Genet 40:335–339.

Shimomura Y, Wajid M, Petukhova L, Shapiro L, Christiano AM. 2009b. Mutations in the lipase H gene underlie autosomal recessive woolly hair/hypotrichosis. J Invest Dermatol 129:622–628.

Shimomura Y, Wajid M, Zlotogorski A, Lee YJ, Rice RH, Christiano AM. 2009c. Founder mutations in the lipase h gene in families with autosomal recessive woolly hair/hypotrichosis. J Invest Dermatol 129:1927–1934.

Sonoda H, Aoki J, Hiramatsu T, Ishida M, Bandoh K, Nagai Y, Taguchi R, Inoue K, Arai H. 2002. A novel phosphatidic acid-selective phospholipase A1 that produces lysophosphatidic acid. J Biol Chem 277:34254–34263.

Tokumaru S, Higashiyama S, Endo T, Nakagawa T, Miyagawa JI, Yamamori K, Hanakawa Y, Ohmoto H, Yoshino K, Shirakata Y, Matsuzawa Y, Hashimoto K, Taniguchi N. 2000. Ectodomain shedding of epidermal growth factor receptor ligands is required for keratinocyte migration in cutaneous wound healing. J Cell Biol 151:209–220.

Wali A, Chishti MS, Ayub M, Yasinzai M, Kafaitullah, Ali G, John P, Ahmad W. 2007. Localization of a novel autosomal recessive hypotrichosis locus (LAH3) to chromosome 13q14.11–q21.32. Clin Genet 72:23–29.

Whittock NV, Bower C. 2003. Genetic evidence for a novel human desmosomal cadherin, desmoglein 4. J Invest Dermatol 120:523–530.

Xu X, Quiros RM, Gattuso P, Ain KB, Prinz RA. 2003. High prevalence of BRAF gene mutation in papillary thyroid carcinomas and thyroid tumor cell lines. Cancer Res 63:4561–4567.

severe chronic upper airway disease (SCUAD). J Allergy Clin Immunol 2009;124: 428-33.
4. Okano M, Fujiwara T, Haruna T, Kariya S, Makihara S, Higaki T, et al. PGE_2 suppresses staphylococcal enterotoxin-induced eosinophilia-associated cellular responses dominantly via an EP2-mediated pathway in nasal polyps. J Allergy Clin Immunol 2009;123:868-74.
5. Bachert C, Zhang N, van Zele T, Gevaert P, Patou J, van Cauwenberge P. *Staphylococcus aureus* enterotoxins as immune stimulants. In: Halilos DL, Baroody FM, editors. Chronic rhinosinusitis. Pathogenesis and medical management. New York: Informa Healthcare USA; 2007. p. 163-75.
6. Napolitani G, Acosta-Rodriguez EV, Lanzavecchia A, Sallusto F. Prostaglandin E_2 enhances Th17 responses via modulation of IL-17 and IFN-γ production by human CD4+ T cells. Eur J Immunol 2009;39:1-12.
7. Saito T, Kusunoki T, Yao T, Kawano K, Kojima Y, Miyahara K, et al. Role of interleukin-17A in the eosinophil accumulation and mucosal remodeling in chronic rhinosinusitis with nasal polyps associated with asthma. Int Arch Allergy Immunol 2009;151:8-16.
8. Su YC, Rolph MS, Hansbro NG, Mackay CR, Sewell WA. Granulocyte-macrophage colony-stimulating factor is required for bronchial eosinophilia in a murine model of allergic airway inflammation. J Immunol 2008;180:2600-7.
9. Doganci A, Eigenbrod T, Krug N, De Sanctis GT, Hausding M, Erpenbeck VJ, et al. The IL-6R alpha chain controls lung CD4+CD25+ Treg development and function during allergic airway inflammation in vivo. J Clin Invest 2005; 115:313-25.

Available online July 12, 2010.
doi:10.1016/j.jaci.2010.05.014

Topical application of dehydroxymethylepoxyquinomicin improves allergic inflammation via NF-κB inhibition

To the Editor:

Atopic dermatitis (AD) is a chronic, relapsing inflammatory skin disease with significant morbidity and an adverse impact on patient well-being. AD has become increasingly prevalent in industrialized countries, where it now occurs in 10% to 20% of children and 1% to 3% adults.[1] Corticosteroids are generally prescribed to control the symptoms, yet repeated use can cause severe skin atrophy and susceptibility to infection.[2] Tacrolimus, a calcineurin inhibitor, has recently gained widespread use as an AD treatment that avoids the typical side effects associated with topical corticosteroids.[3] However, refractory AD can remain even in patients treated with both corticosteroid and tacrolimus.

Dehydroxymethylepoxyquinomicin (DHMEQ), a newly developed low-molecular-weight nuclear factor- κB (NF-κB) inhibitor, is a 5-dehydroxymethyl derivative of the antibiotic epoxyquinomicin C.[4] DHMEQ has been found to inhibit TNF-α–induced NF-κB activation by suppressing nuclear translocation but not IκB phosphorylation or degradation.[5] Recently the antitumor effects of DHMEQ on breast,[6] thyroid,[7] and prostate[8] cancers as well as its anti-inflammatory and immunosuppressive effects have been reported in mice models.[9,10] In this study, we used atopic dermatitis model mice to examine the antiallergic inflammation efficacy of DHMEQ.

We confirmed that DHMEQ effectively inhibited the NF-κB activity in macrophage-like cell line, RAW264.7 with LPS stimulation (Fig 1, *A*).

First we examined whether DHMEQ suppressed contact hypersensitivity response. Balb/c mice were sensitized with 2,4,6-trinitrochlorobenzene (TNCB) to the dorsal skin and challenged 5 days later on the dorsal surface of the right ear. Immediately after the challenge, DHMEQ (1 mg/mL in acetone) or tacrolimus ointment (1%) was applied to the same ear. The DHMEQ-treated ears showed significantly less ear swelling than the tacrolimus-treated ears (Fig 1, *B*). The suppressive effect of DHMEQ was dose-dependent (Fig 1, *C*). Furthermore, expression of inflammatory cytokine mRNA (IL-1β, IL-6, TNF-α) in lesional skin was suppressed by DHMEQ ointment as well as by tacrolimus ointment (Fig 1, *D*). These data show that DHMEQ suppresses inflammation via suppression of inflammatory cytokine expression regulated by NF-κB.

We next examined whether DHMEQ would inhibit hapten-induced Langerhans cell (LC) migration. Treatment with TNCB caused a significant decline in epidermal LC density 4 hours after application in the untreated mice (30.5%). In contrast, TNCB treatment failed to provoke a significant epidermal LC migration response in the DHMEQ-treated mice (13.1%; Fig 1, *E*). We further evaluated LC morphology in the epidermal sheet preparations derived from the untreated and DHMEQ-treated mice. As illustrated in Fig 1, *F (left)*, at 4 hours after exposure to TNCB, the LCs in the control mice appeared to be activated and to have extended dendritic processes, whereas no such morphologic changes were evident in the LCs examined in the DHMEQ-treated mice (Fig 1, *F, right*). These data support that the DHMEQ suppressed the contact hypersensitivity response at least in part by inhibition of LC migration.

To determine whether DHMEQ has any therapeutic effect in AD, we applied DHMEQ to AD-like lesions of NC/Nga mice and evaluated the progression of skin changes. NC/Nga mice were the spontaneous mouse models of AD. Another spontaneous mouse model, the DS-Nh mouse, has a mutation of transient receptor potential vanilloid 3,[11] whereas the genetic defect of NC/Nga is not known. We used conventional NC/Nga mice that presented severe skin lesions very similar to those of human AD.[12] Conventional NC/Nga mice with moderate to severe AD were topically applied with 1% DHEMQ in plastibase (5% polyethylene and 95% mineral oil), 0.1% tacrolimus ointment, or 0.12% betamethasone ointment daily for 2 weeks. The clinical severity of skin lesion was scored daily according to the 5 main clinical symptoms: scratch behavior, erythema/hemorrhaging, edema, excoriation/erosion, and scaling/dryness.[12] Topical DHMEQ application significantly improved the severity of skin lesions compared with the ointment base as well compared with topical treatment with the 0.1% tacrolimus or 0.12% betamethasone ointment (Fig 2, *A and B*). Improvement of clinical skin condition by DHMEQ was also confirmed by histologic observation, which showed amelioration of hyperkeratosis, acanthosis, dermal edema, and infiltration of the inflammatory cells compared with the ointment base treatment (Fig 2, *C*). At the affected skin sites, the numbers of eosinophils and mast cells were significantly lower in the DHMEQ-treated mice than those in the control mice (Fig 2, *C*).

Potential side effects of topical application of NF-κB inhibition might include susceptibility to infection via local immune suppression. However NF-κB inhibitor presumably avoids the typical side effects associated with topical corticosteroids as well as tacrolimus.

Several reagents targeting NF-κB have been reported. For example, NF-κB decoy oligodeoxynucleotides were reported to be effective in resolving atopic skin lesions in NC/Nga mice.[13] IMD-0354, a selective IKK inhibitor, also improved AD manifestation in model mice.[14] In contrast with these, DHMEQ inhibits NF-κB activation by suppressing nuclear translocation but not IκB phosphorylation or degradation.[5] Because DHMEQ has a unique mechanism to inhibit NF-κB activation, DHMEQ might be effective for AD that does not respond to tacrolimus or corticosteroid, and it might have additive effects with other reagents.

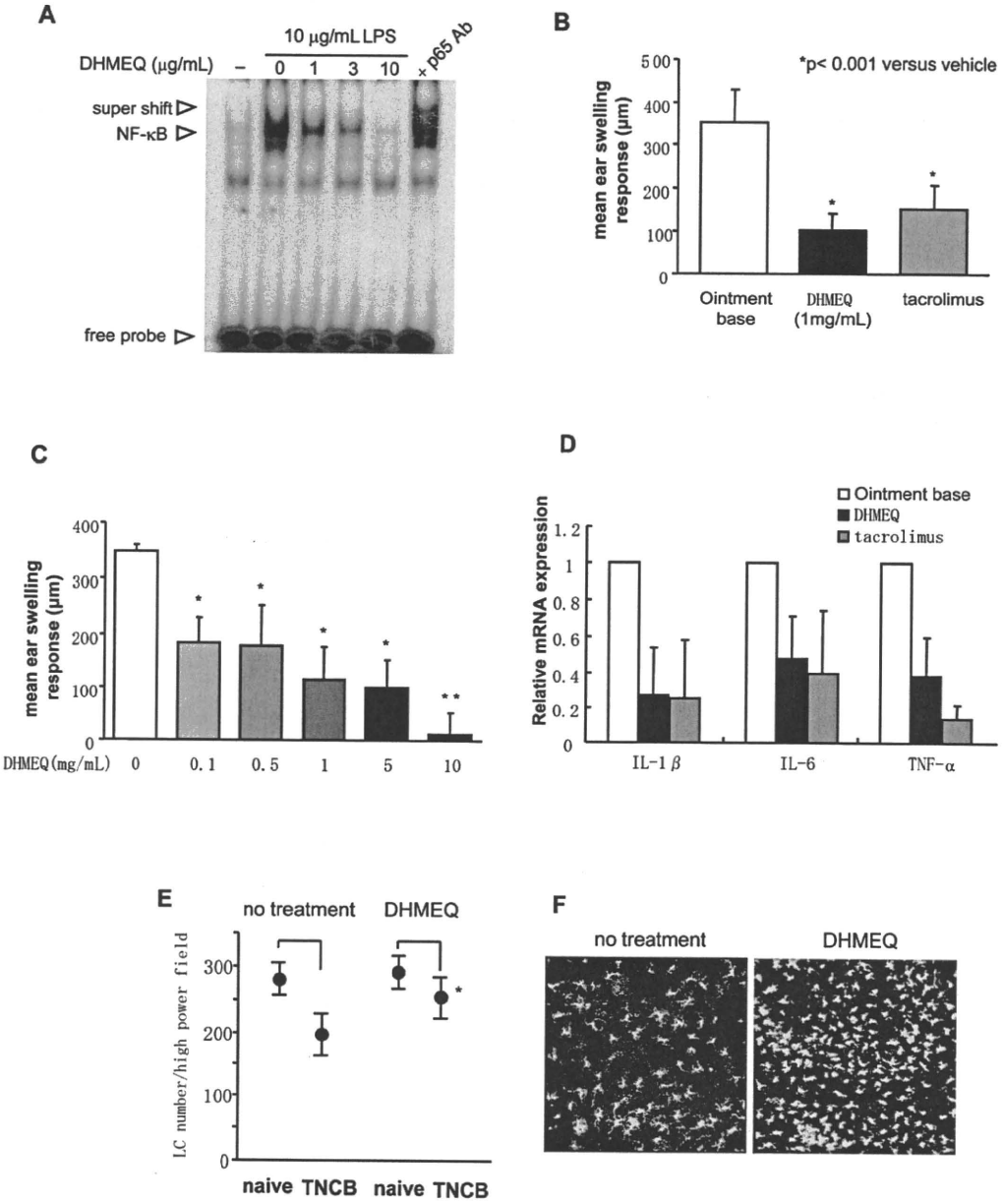

FIG 1. Effect of DHMEQ on contact hypersensitivity response. **A,** DHMEQ effectively inhibited the NF-κB activity in macrophagelike cell line RAW264.7 with LPS stimulation (10 μg/mL). **B,** DHMEQ, tacrolimus, or ointment base was applied topically. All ear-swelling values are shown as means ± SEs (n = 5). $*P < .01$; $**P < .005$. **C,** DHMEQ was applied in various concentrations. **D,** The density of mRNA expression of skin was analyzed by RT-PCR. **E,** The number of LCs was counted. $*P < .05$ (n = 4 for each group). **F,** LC morphology in epidermal sheet preparations derived from untreated *(left)* and DHMEQ-treated *(right)* mice.

In conclusion, we clearly demonstrated that DHMEQ inhibits the contact hypersensitivity response via suppression of inflammatory cytokines and decrease in LC migration. Furthermore, DHMEQ was found to improve AD manifestation of model mice with an efficacy equivalent to that of tacrolimus or betamethasone. DHMEQ may offer a novel therapeutic approach for the treatment of AD.

Asuka Hamasaka, MD, PhD[a]*
Naoya Yoshioka, MS[a]*
Riichiro Abe, MD, PhD[a]
Satoshi Kishino, PhD[d]
Kazuo Umezawa, MD, PhD[e]
Michitaka Ozaki, MD, PhD[b]
Satoru Todo, MD, PhD[c]
Hiroshi Shimizu, MD, PhD[a]

From [a]the Department of Dermatology, [b]the Department of Molecular Surgery, and [c]the First Department of Surgery, Hokkaido University Graduate School of Medicine, Sapporo; [d]the Department of Medication Use Analysis and Clinical Research, Meiji Pharmaceutical University, Tokyo; and [e]the Department of Applied Chemistry, Keio

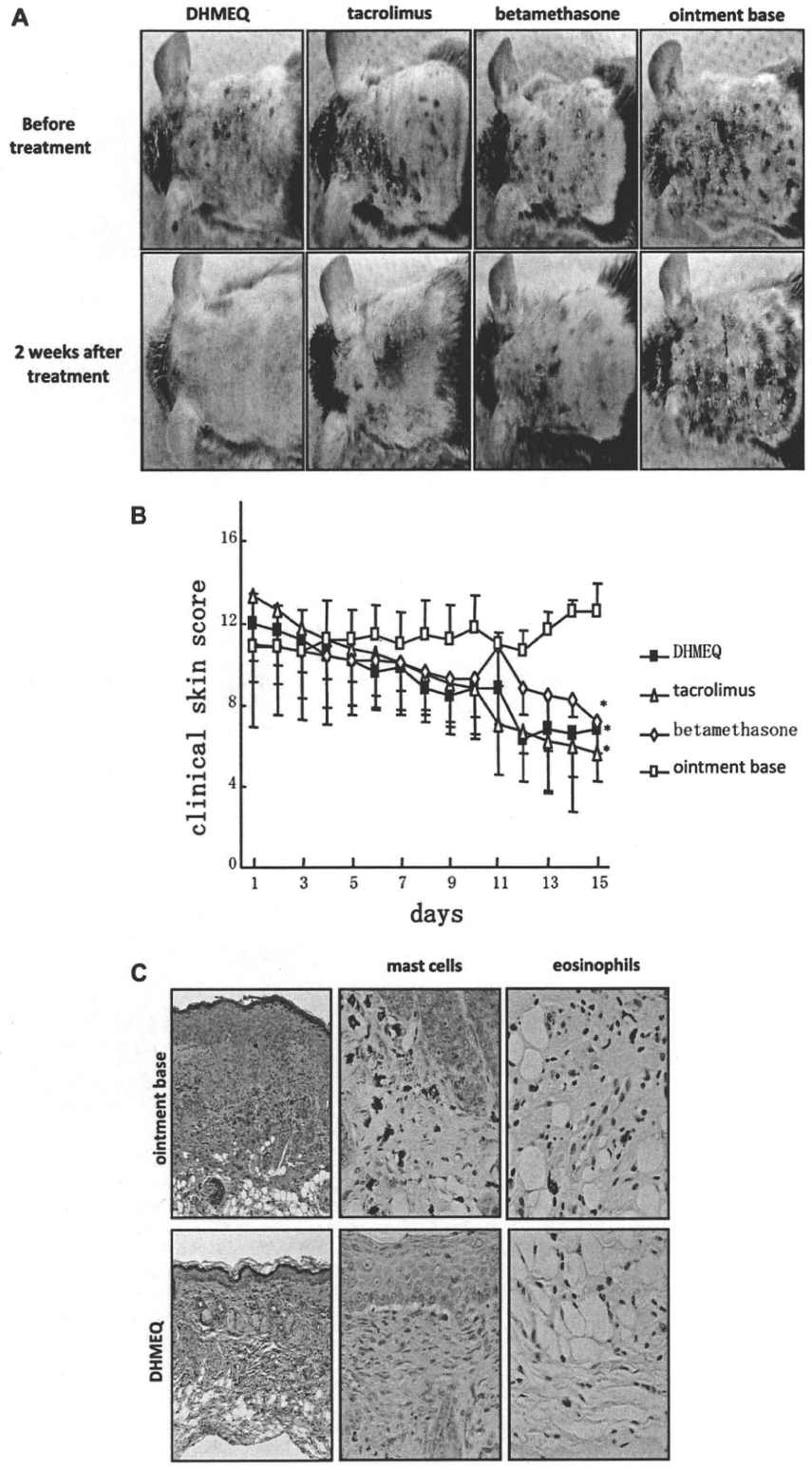

FIG 2. Improvement of atopic dermatitis model mice by DHMEQ. NC/Nga mice were applied topically with DHMEQ, tacrolimus, or ointment base. **A,** Clinical features of each mouse. **B,** The clinical skin score of each group is given as mean ± SE. *$P < .005$. **C,** Specimens were collected from the dorsal skin and were stained with hematoxylin and eosin, direct fast scarlet for eosinophils, or toluidine blue for mast cells.